Chapter 3: Effects of solvent exchange on the dynamic motions of $(Me_2NH_2)[In(ABDC)_2]$

3.1 Abstract

The dynamic responses of $(Me_2NH_2)[In(ABDC)_2]$ to exchange and removal of different solvent systems are explored using a combination of single crystal and powder X-ray diffraction techniques. The results reveal a large solvent dependence in the flexibility of the framework, which appears to be based on the solvent polarity. A further flexibility of the framework, different to the continuous breathing behaviour explored in chapter 2 is also discovered, involving a defined phase transition, and a substantial change to the coordination environment of the indium centres.

3.2 Introduction

Solvent exchange is a common precursor in the activation (solvent removal) of MOF materials, allowing the often high-boiling point solvents typically used in the synthesis to be exchanged for more volatile (and weakly interacting solvents) that can be removed more easily.[1–6] This method was adopted in the original report of $(Me_2NH_2)[In(ABDC)_2]$, which explored the volumetric gas uptake properties of the framework after solvent removal from a $CHCl_3$-exchanged sample.[7] The effect of solvent exchange is particularly relevant in flexible frameworks, which can exist in different stable phases while containing different guests. [8–10] Work for example on MCF-18 ($[M_3(\mu\text{-OH})(DCPBP)_3]$[9] (DCPBP = 2,6-di-*p*-carboxyphenyl-4-4'-bipyridine) and $[In_2(OH)_2(obb)_2]$[10] (obb = 4,4'-oxybis(benzoate)) show large changes to the observed PXRD patterns after soaking the frameworks in a wide range of guests. The guests included water, alcohols, DMF and small cyclic organic compounds, and was coupled with a change in the degree of pore opening due to a change in the intermolecular interactions. Similar effects have been observed for the well-known MIL-53 framework displaying a range of different unit cell parameters while containing differing guests, due to variations in the degree of pore opening.[11–13] The effect of solvent exchange for MIL-53 was studied in detail by Millange, Walton and co-workers using *in situ* diffraction techniques.[8, 14] These experiments used energy dispersive X-ray diffraction to follow the structural evolution upon dropwise introduction of guest molecules to a sample of hydrated MIL-53 suspended in water. The addition of the guests was coupled with an immediate introduction of a new crystalline phase. The ratios of Bragg reflections of the new phase and the initial phase changed over time as increasing amounts of guests were adsorbed. No evidence of intermediate phases was seen except in the case

methanol adsorption where a defined transition to an intermediate transient phase, whose Bragg reflections then shifted slightly during the experiment was observed, before another transition to the fully solvated from. [8, 14] The final fully exchanged structures were seen to vary dramatically based on the guest, but followed a consistent trend related to the opening and closing of the lozenge shaped channels. For more information related to this the reader is directed to chapter 1. The results from these MOFs show the large structural changes that can occur due to differing guest inclusion, but also show they mostly appear to be limited to displaying a single phase while containing any one solvent. Work in the previous chapter has shown that $(Me_2NH_2)[In(ABDC)_2]$ instead displays a rare continuous breathing mechanism where the degree of opening is highly variable, and strongly linked to the amount of contained solvent. Little is currently known in the literature about this sort of flexibility or the effect different solvents have on the dynamic motions. These effects will be explored in the chapter using the three common laboratory solvents: acetone, THF and $CHCl_3$. These solvents were selected to provide a polar solvent alternative to DMF, namely acetone, and two different less polar solvents. The behaviour of the MOF on removal of $CHCl_3$ from a solvent exchanged framework is of particular relevance, due to the reported volumetric gas adsorption results.

3.3 Experimental

3.3.1 General

All reagents were purchased from Sigma-Aldrich or Alfa Aesar and were used without further purification, unless otherwise stated.

3.3.2 Synthesis

Synthesis of acetone-exchanged MOF $[In(ABDC)_2Me_2NH_2]$

Single crystals of as-synthesised $(Me_2NH_2)[In(ABDC)_2]$ (50 mg, 0.01 mmol) were placed in HPLC grade acetone (1 mL), dried over 4Å molecular sieves, for 1 week. Acetone was replaced daily.

Synthesis of tetrahydrofuran (THF)-exchanged MOF $[In(ABDC)_2Me_2NH_2]$

Single crystals of as-synthesised $(Me_2NH_2)[In(ABDC)_2]$ (50 mg, 0.01 mmol) were placed in THF (1 mL), dried according to the method of Grubbs,[15] for 1-2 weeks. THF was replaced daily.

Synthesis of chloroform $(CHCl_3)$-exchanged MOF $[In(ABDC)_2Me_2NH_2]$

Single crystals of as-synthesised $(Me_2NH_2)[In(ABDC)_2]$ (50 mg, 0.01 mmol) were placed in $CHCl_3$ (1 mL), dried according to the method of Grubbs,[15] for 1-2 weeks. $CHCl_3$ was replaced daily.

3.3.3 Analysis

TGA analyses were obtained using a Perkin Elmer Thermogravimetric Analyser under a nitrogen atmosphere. The sample (3.3 mg) was held at 25 ^oC for 30 minutes prior to heating from 25^oC to 600^oC at a rate of 4 ^oC/min. The exported data were plotted using Microsoft Excel.

Solution-phase ^1H NMR spectroscopy (400MHz, DMSO-d6) was carried out using a Bruker DPX-400 spectrometer. The MOF sample (10 mg) was digested using 50 µL of acid (35% DCl in D_2O) in 1 ml of DMSO-d6, and recorded without neutralising the solution. All the constituent parts were observed to be soluble in the DMSO after the digestion.

Single Crystal X-ray Diffraction

Laboratory single-crystal X-ray diffraction data were collected on a Bruker SMART APEX-II CCD diffractometer operating a Mo-K_α sealed-tube X-ray source or a Bruker D8 Venture diffractometer equipped with a PHOTON 100 dual-CMOS chip detector and operating a Cu-K_α IµS microfocus X-ray source. The data were processed using the APEX2 software.[16] X-Ray data were corrected for

absorption using empirical methods (SADABS) based upon symmetry-equivalent reflections combined with measurements at different azimuthal angles.[17, 18] An Oxford Cryosystems Cryostream device was to maintain the sample temperature. Synchrotron diffraction data were recorded at beamline I19[19] at Diamond Light Source. A full hemisphere of data was collected using three 132 °, and one 180 ° omega scans at 0.4 ° slicing on a Newport diffractometer equipped with a Pilatus 300K detector. Data were recorded at a wavelength of 0.6889(1) Å, took 15 min to collect and were processed and corrected for adsorption using Agilent Crysalis Pro software. All crystal structures were solved and refined against F^2 values using the SHELX 2013 suite accessed within the OLEX2 program.[20, 21] Non-disordered, non-hydrogen framework atoms were refined anisotropically, but disordered framework atoms and cations were modelled with isotropic displacement parameters, using a combination of crystallographic restraints and constraints. Hydrogen atoms were placed in calculated positions with idealised geometries and then refined using a riding model with isotropic displacement parameters. Final CIFs were checked using checkCIF/PLATON.[22] PLATON SQUEEZE was used to obtain a residual electron count within the pore, but was not used in the structure refinements.[23] The routine SQUEEZE in the program PLATON was used to obtain a residual electron count within the pore.[23] All electron counts were obtained after fully removing any modelled counter ions from the crystallographic model and re-refining the structure. The electron count related to solvent was then determined by manually subtracting to number of electron associated with the counter ions from the total contained within the unit cell.

Powder X-ray Diffraction

Laboratory powder diffraction data were obtained using a Bruker D8 Advance powder diffractometer equipped with focusing Göbel mirrors, recorded in the range $4\ ^{o} \leq 2\theta \leq 50\ ^{o}$, using Cu-$K_\alpha$ radiation. Data were collected in a Debye-Scherrer geometry with rotating capillary stage and samples loaded in either 0.5 mm or 0.7 mm borosilicate capillaries. Sample temperature for *in situ* heating studies was controlled by a co-axial stream of dry nitrogen gas from an Oxford Cryosystems Cryostream Plus device, with a flow rate of 5 L/min. Synchrotron powder diffraction data were collected at beamline I11 at Diamond Light Source using a wide-angle (90 °) position sensitive detector (PSD) comprising 18 Mythen-2 modules.[24, 25] A pair of scans related by a 0.25 ° detector offset was collected for each measurement to account for gaps between detector modules. The resulting patterns were summed to give the final pattern for analysis. All ambient pressure data were collected in transmission geometry using either 0.5 or 0.7 mm diameter borosilicate capillaries. Indexing, Pawley and Rietveld refinements were carried out using TOPAS version 4.1[26–31]

Measures of agreement between the calculated and experimental diffraction data (R_{wp} and R_{wp}') are defined by the equations below.

$$R_{wp} = \sqrt{\frac{\Sigma[w(Y_{\text{obs}} - Y_{\text{calc}})^2]}{\Sigma[wY_{\text{obs}}{}^2]}} \qquad R_{wp}{}' = \sqrt{\frac{\Sigma[w(Y_{\text{obs}} - Y_{\text{calc}})^2]}{\Sigma[w(Y_{\text{obs}} - bkgr)^2]}}$$

3.3.4 Crystallographic studies of acetone-exchanged $(Me_2NH_2)[In(ABDC)_2]$

Attempts to obtain a crystal structure of acetone-exchanged $(Me_2NH_2)[In(ABDC)_2]$

Single crystals of $(Me_2NH_2)[In(ABDC)_2]$ obtained after exchange of DMF for acetone were directly transferred into a perfluoropolyether oil (FOMBLIN Y). The crystals (**A1-5**) were mounted onto MiTeGen 200µm MicroMounts under an optical microscope, and transferred to the diffractometer and immersed in the dry nitrogen stream of the Cryostream device at 100 K. All the crystals diffracted well and unit cell cells could be convincingly determined from the diffraction data, however, analysis of relevant systematic absences suggested no suitable space group. Charge flipping algorithms were used to solve the structure in space group *P*1 and determine the relevant symmetry from the phases of the solved crystal structure afterwards. The solutions suggested space group *Fddd*, consistent with crystal structures of the as-synthetized material. The least-squares refinements of the structure in space group *Fddd* were stable and the framework atoms could be located, but showed high R1 and wR2 values due to high electron density peaks in the pore which could not be suitably modelled either as solvent molecules or Me_2NH_2 cations. The contribution of the electron density of these molecules could however be accounted for using the SQUEEZE routine with the program PLATON.[23] The crystal structure parameters can be seen in Table 2.

The precession images of the diffraction patterns (**A1-5**) were analysed. The images showed satellite peaks and suggested modulation effects. The 0kl, h0l and hk0 planes of **A3** are shown in Figure 1. It is currently unknown if the structures are commensurately or incommensurately modulated, and no structure solutions taking into account modulation have been attempted.

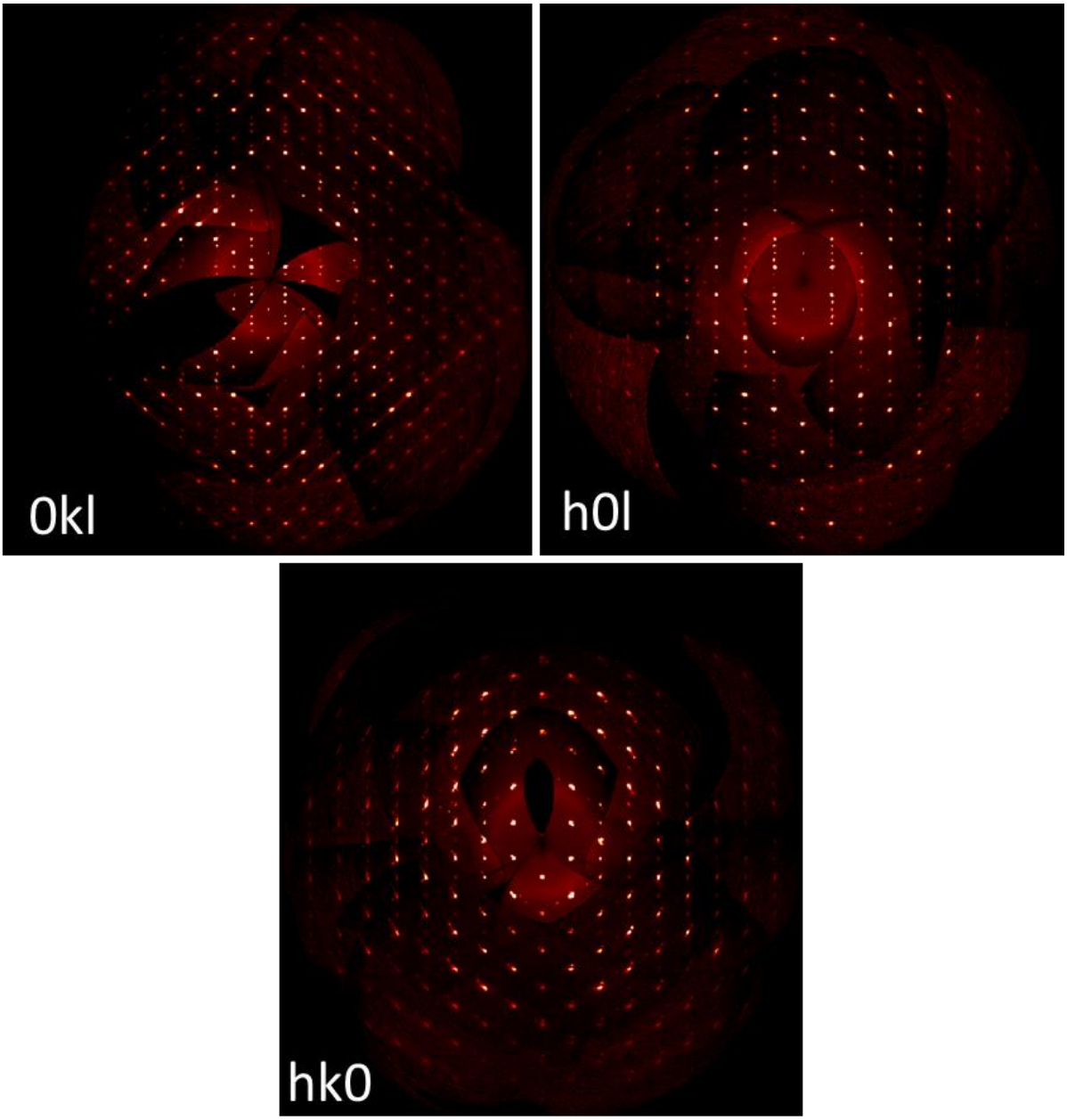

Figure 1 - Precession images of the 0kl, h0l and hl0 planes in acetone-exchanged $(Me_2NH_2)[In(ABDC)_2]$ **A3**

In situ heating experiments

Crystals used for *in situ* heating were selected while immersed in acetone, and one face of the crystal was glued to a glass fibre while the crystal was still covered in a thin layer of residual solvent. Care was taken to avoid coating the entire crystal in adhesive. The crystal was rapidly transferred to the diffractometer and situated in the nitrogen stream of the Cryostream device at room temperature. The glue was left to dry for 15 mins before any data were collected. Heating was carried out *in situ* using the Cryostream device. Two different heating experiments were carried out

on two separate crystals (**A6** and **A7**). A ramp rate of 4 °C/min was used to raise the temperature, which was held at the final value for a fixed period (see Table 1) before cooling at a ramp rate of 4 °C/min. Intensity data collections were recorded under the nitrogen stream at 298 K, using the Cryostream to maintain the temperature. The unit cell parameters were obtained by analysing reflections of I/σ > 10 from 4 sets of 10° omega scans with 0.5° slicing. A full data collection was recorded at the end of the study 1 (**A6.4**) after cooling the crystal to 100 K. This structure solution showed little evidence of satellite peaks in the precession images and showed appropriate systematic absences for the space group *Fddd*. Table 1 details the two separate heating studies carried out and the resulting unit cell parameters. The details of the full data collection **A6.4** is shown in Table 3, and Figure 2 and Figure 3 show the behaviour compared to the observed single crystal breathing trend line of the as-synthesised framework (crystals **1-10** in chapter 2).

Table 1 - Parameters used and unit cell determined for crystallographic studies of desolvation by *in situ* heating

Heating Study No.	Temp heated	Hold time	Data Set Code	*a* (Å)	*b* (Å)	*c* (Å)	*V* (Å^3)
1	25 °C	Start	**A6.1**[a]	15.16(1)	24.30(2)	33.31(2)	12270(17)
	60 °C	5 mins	**A6.2**[a]	15.15(1)	23.01(2)	34.12(2)	11890(20)
	80 °C	15 mins	**A6.3**[a]	15.41(1)	21.41(1)	34.83(2)	11490(12)
	Cooled to 100K		**A6.4**[b]	15.706(2)	21.101(2)	34.882(4)	11560(2)
2	25 °C	Start	**A7.1**[a]	15.38(1)	21.71(1)	34.68(2)	11579(12)
	40 °C	5 mins	**A7.2**[a]	15.418(5)	21.300(6)	34.95(1)	11477(6)
	60 °C		**A7.3**[a]	15.386(6)	21.257(7)	34.5(1)	11430(7)
	80 °C		**A7.4**[a]	15.250(9)	21.73(4)	34.71(2)	11504(20)

[a] Data collection at 298 K after heating cycle

[b] Data collection at 100 K

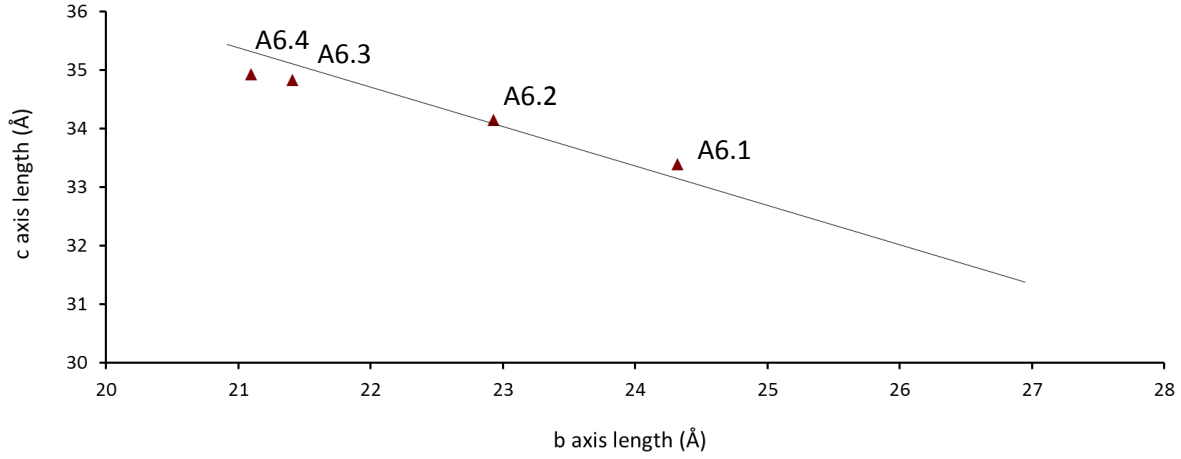

Figure 2 - Results of *in situ* heating experiment 1 on acetone-exchanged $(Me_2NH_2)[In(ABDC)_2]$ (**A6.1-6.4**) in comparison to the trend line from single crystal desolvation studies of as-synthesised $(Me_2NH_2)[In(ABDC)_2]$ (**1-10**)

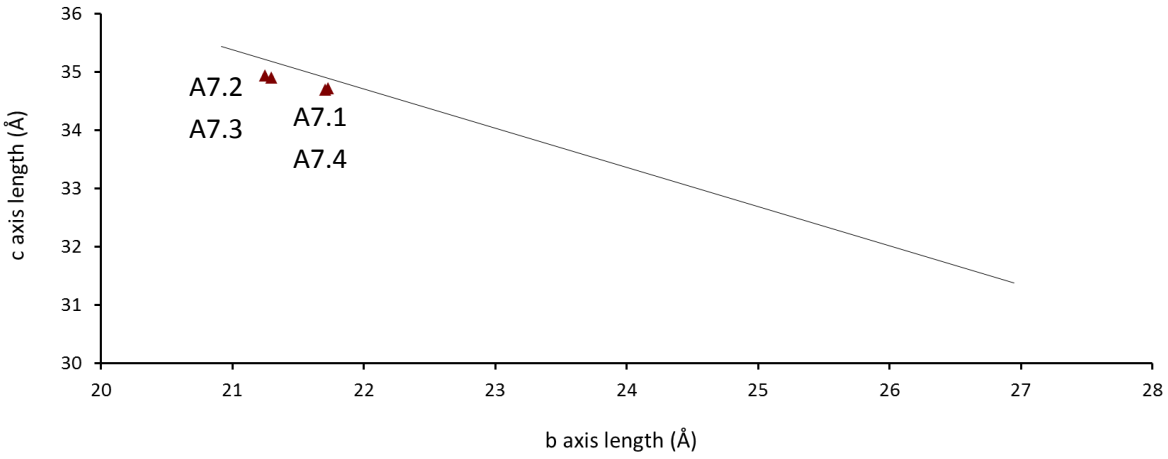

Figure 3 - Results of *in situ* heating experiment 2 on acetone-exchanged $(Me_2NH_2)[In(ABDC)_2]$ (**A7.1-7.4**) in comparison to the trend line from single crystal desolvation studies of as-synthesised $(Me_2NH_2)[In(ABDC)_2]$ (**1-10**)

Table 2 - Data collection, structure solution and refinement parameters for single crystal X-ray structure determinations of acetone-exchanged MOF $(Me_2NH_2)[In(ABDC)_2]$

	Acetone-exchanged MOF -1 **(A1)**	Acetone-exchanged MOF -2 **(A2)**	Acetone-exchanged MOF -3 **(A3)**
Crystal Habit	Octahedron	Octahedron	Octahedron
Crystal Colour	Brown	Brown	Brown
Crystal Size (mm)	0.15 × 0.15 × 0.15	0.34 × 0.24 × 0.23	0.35 × 0.25 × 0.17
Crystal System	Orthorhombic	Orthorhombic	Orthorhombic
Space Group, Z	*Fddd*, 16	*Fddd*, 16	*Fddd*, 16
a (Å)	15.1385(6)	15.1258(7)	15.005(6)
b (Å)	25.3228(11)	24.7950(11)	24.452(10)
c (Å)	32.5481(11)	32.9741(14)	33.176(13)
α (°)	90	90	90
β (°)	90	90	90
γ (°)	90	90	90
V (Å^3)	12477.3(8)	12366.7(10)	12172(8)
Radiation	Cu-K_α (λ = 1.54178 Å)	Mo-K_α (λ = 0.71073 Å)	Cu-K_α (λ = 1.54178 Å)
Density (g cm^{-3})[b]	1.106	1.116	1.134
Temperature (K)	100	100	100
μ (mm^{-1})[c]	6.312	0.798	6.517
2θ Range (°)	7.32 to 133.86	3.39 to 55.12	7.4 to 134.88
Reflns collected	27336	3570	14040
Independent reflns (R_{int})	2759 (0.0510)	3570 (0.0490)	2712 (0.0509)
Reflns used in refinement, *n*	2759	3570	2712
L.S. parameters, *p*	89	94	89
No. of restraints, *r*	52	0	47
Completeness	0.991	0.996	0.986
$R1(F)$[a] $I > 2\sigma(I)$	0.1602	0.1446	0.1703
$wR2(F^2)$[a], all data	0.4090	0.3828	0.4224
$S(F^2)$[a], all data	1.289	1.229	1.235

[a] $R1(F) = \sum(|F_o| - |F_c|)/\sum|F_o|$; $wR2(F^2) = \sqrt{\sum w\left(F_o^2 - F_c^2\right)^2/\sum wF_o^4}$; $S(F^2) = \sqrt{\sum w\left(F_o^2 - F_c^2\right)^2/(n+r-p)}$.

[b] Densities are calculated using only framework atoms and cations, and do not include guest molecules.

[c] Adsorption coefficients are calculated based on the crystallographic model

Table 3 – Data collection, structure solution and refinement parameters for single crystal X-ray structure determinations of acetone exchanged MOF $(Me_2NH_2)[In(ABDC)_2]$

	Acetone-exchanged MOF - 4 **(A4)**	Acetone-exchanged MOF - 5 **(A5)**	*In situ* heating of acetone-exchanged MOF -1 **(A6.4)**
Crystal Habit	Octahedron	Octahedron	Octahedron
Crystal Colour	Brown	Brown	Brown
Crystal Size (mm)	0.33 × 0.23 × 0.2	0.4 × 0.27 × 0.17	0.40 × 0.20 × 0.19
Crystal System	Orthorhombic	Orthorhombic	Orthorhombic
Space Group, Z	*Fddd*, 16	*Fddd*, 16	*Fddd*, 16
a (Å)	14.925(10)	15.0363(9)	15.706(2)
b (Å)	24.033(16)	23.5811(16)	21.101(2)
c (Å)	33.47(3)	33.7840(19)	34.882(4)
α (°)	90	90	90
β (°)	90	90	90
γ (°)	90	90	90
V (Å^3)	12006(15)	11978.9(13)	11560(2)
Radiation	Cu-K_α (λ = 1.54178 Å)	Cu-K_α (λ = 1.54178 Å)	Cu-K_α (λ = 1.54178 Å)
Density (g cm^{-3})[b]	1.149	1.152	1.194
Temperature (K)	100	100	100
μ (mm^{-1})[c]	6.560	6.575	6.862
2θ Range (°)	7.46 to 133.96	7.45 to 133.82	7.46 to 134.26
Reflns collected	12189	11529	11780
Independent reflns (R_{int})	2661 (0.0460)	2582 (0.0469)	2517 (0.0637)
Reflns used in refinement, *n*	2661	2582	2517
L.S. parameters, *p*	87	94	141
No. of restraints, *r*	21	11	3
Completeness	0.990	0.964	0.970
$R1(F)$[a] $I > 2\sigma(I)$	0.1634	0.1240	0.0965
$wR2(F^2)$[a], all data	0.4117	0.3282	0.2691
$S(F^2)$[a], all data	1.271	1.244	1.080

[a] $R1(F) = \sum(|F_o| - |F_c|)/\sum|F_o|$; $wR2(F^2) = \sqrt{\sum w\left(F_o^2 - F_c^2\right)^2/\sum wF_o^4}$; $S(F^2) = \sqrt{\sum w\left(F_o^2 - F_c^2\right)^2/(n+r-p)}$.

[b] Densities are calculated using only framework atoms and cations, and do not include guest molecules.

[c] Adsorption coefficients are calculated based on the crystallographic model

SQUEEZE analysis

The electron density in the pore of the material, which was unable to be modelled, was accounted for by the routine SQUEEZE[23] in the program PLATON, [22] following the procedure detailed in section 3.3.3. The crystal structures were further refined using the solvent free hkl file written by the routine. The results of the analysis are shown in Table 4. The number of electrons per cell corresponds to both solvent and cations, with the number of electrons due to solvent being determined by subtracting the number of electrons associated with the cation and dividing by the number of formula units within one unit cell. The R factors shown are for refinement against the solvent free hkl and show significant improvements compared to the normal solvent contained hkl (*cf*. Table 2 and Table 3).

Table 4 – Electron count and refinement parameters during SQUEEZE analysis of acetone-exchanged MOF $(Me_2NH_2)[In(ABDC)_2]$

	Electrons per unit cell (in void spaces)	Solvent accessible void per unit cell (Å^3)	Electrons per Indium due to solvent [b]	$R1(F)$[a] $I > 2\sigma(I)$	$wR2(F^2)$[a], all data	$S(F^2)$[a], all data
A1	1951	6383.8	95	0.0884	0.2149	1.166
A2	1803	6493.8	86	0.0842	0.2118	1.094
A3	1662	5949.0	77	0.1025	0.2381	1.160
A4	1591	5901.9	72	0.0975	0.2326	1.199
A5	1692	6064.9	79	0.0666	0.1571	1.129
A6.4	1382	5736.1	60	0.0655	0.1934	1.113

[a] $R1(F) = \sum(|F_o| - |F_c|)/\sum|F_o|$; $wR2(F^2) = \sqrt{\sum w\left(F_o^2 - F_c^2\right)^2/\sum wF_o^4}$; $S(F^2) = \sqrt{\sum w\left(F_o^2 - F_c^2\right)^2/(n+r-p)}$.

[b] Calculated by dividing the electron count per cell by Z and subtracting the electrons associated with the cations

3.3.5 Crystallographic studies of THF-exchanged $(Me_2NH_2)[In(ABDC)_2]$

Crystal structure of THF-exchanged $(Me_2NH_2)[In(ABDC)_2]$

Single crystals obtained after solvent exchange with THF were directly transferred into a perfluoropolyether oil (FOMBLIN Y). A crystal (**T1**) was mounted onto a MiTeGen 200µm MicroMount under an optical microscope, transferred to the diffractometer and immersed in the dry nitrogen stream of the Cryostream device at 100 K. The crystallographic parameters for data collection and structure solution are listed in Table 6.

In situ heating experiments

Crystals used for *in situ* heating were selected while immersed in THF, and one face of the crystal was glued to a glass fibre while the crystal was still covered in a thin layer of residual solvent. Care was taken to avoid coating the entire crystal in adhesive. The crystal was rapidly transferred to the diffractometer and situated in the nitrogen stream of the Cryostream device at room temperature. The glue was left to dry for 15 mins before any data were collected. Heating was carried out *in situ* using the Cryostream device. Two different heating experiments were carried out on two separate crystals (**T2** and **T3**). A ramp rate of 4 ^{o}C/min was used to raise the temperature, which was held at the final value for a fixed period (see Table 5) before cooling at a ramp rate of 4 ^{o}C/min. Measurements during the experiment were recorded at 298K, using the cryostream to maintain the temperature. The unit cell parameters were obtained by analysing reflections of $I/\sigma > 10$ from 4 sets of 10^{o} omega scans with 0.5^{o} slicing. Full data collections were recorded at the end of the studies (**T2.5** and **T3.3**). Table 5 details the two separate heating studies carried out and the resulting cell parameters. The details of the full data collections at the end of studies 1 and 2 are shown in)

Table **6**. Figure 4 & Figure 5 shows the behaviour compared to the observed single crystal breathing trend of the as-synthesised framework (**1-10** in chapter 2).

Table 5 - Parameters used and unit cell determined for crystallographic studies of desolvation by in situ heating

Heating Study No.	Temp heated	Hold time	Data set Code	*a* (Å)	*b* (Å)	*c* (Å)	*V* (Å^3)
1	25 °C	Start	**T2.1**	15.095(5)	26.77(1)	31.44(1)	12707(9)
	40 °C	5 mins	**T2.2**	15.128(7)	26.98(1)	31.23(2)	12748(10)
	60 °C		**T2.3**	15.188(4)	27.375(7)	30.931(9)	12860(6)
	80 °C		**T2.4**	15.205(4)	27.560(7)	30.767(8)	12893(6)
	150 °C		**T2.5**	15.201(3)	27.482(6)	30.868(6)	12895(4)
2	25 °C	Start	**T3.1**	15.483(3)	27.666(6)	30.635(5)	13124(5)
	60 °C	20mins	**T3.2**	15.388(3)	27.458(7)	30.841(5)	13031(5)
	150 °C		**T3.3**	15.0952(4)	26.7260(7)	31.5195(8)	12716.0(6)

All data were recorded at 298K

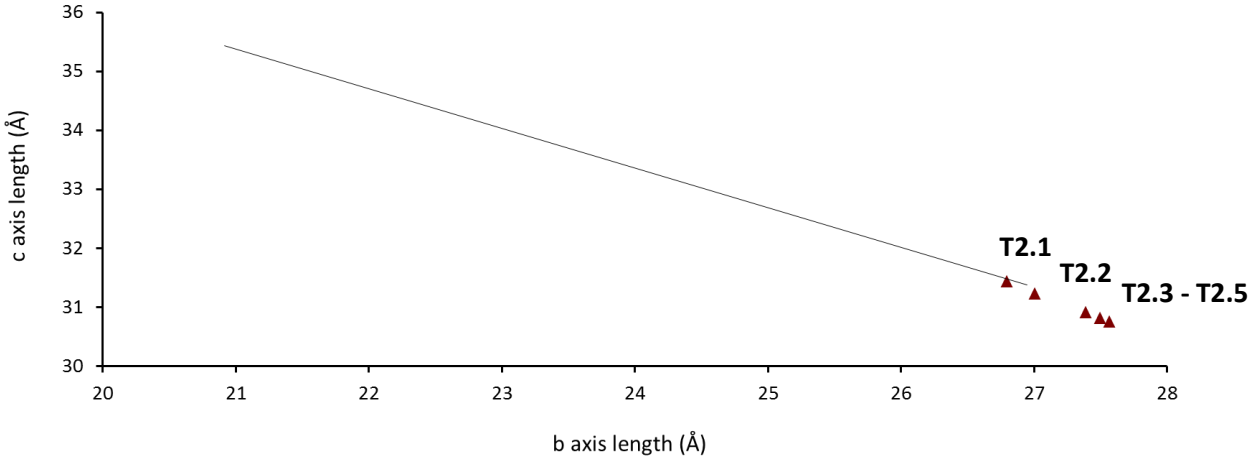

Figure 4 - Results of *in situ* heating experiment 1 on THF-exchanged $(Me_2NH_2)[In(ABDC)_2]$ (**T2.1-2.5**) in comparison to the trend line from single crystal desolvation studies of as-synthesised $(Me_2NH_2)[In(ABDC)_2]$ (**1-10**)

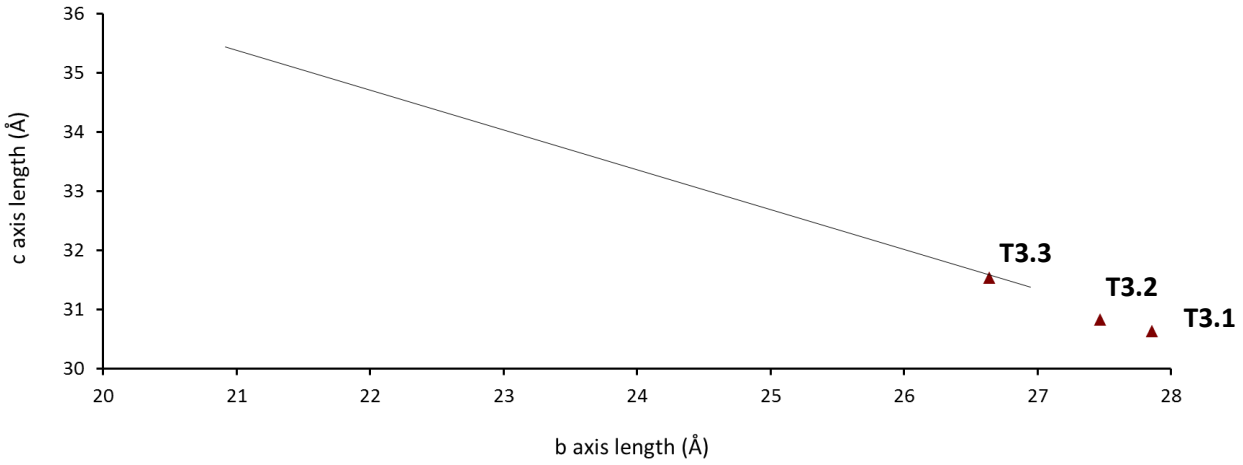

Figure 5 - Results of *in situ* heating experiments 2 on THF-exchanged $(Me_2NH_2)[In(ABDC)_2]$ (**T3.1-3.3**) in comparison to the trend line from single crystal desolvation studies of as-synthesised $(Me_2NH_2)[In(ABDC)_2]$ (**1-10**)

Table 6 - Data collection, structure solution and refinement parameters for single crystal X-ray structure determinations of THF-exchanged MOF $(Me_2NH_2)[In(ABDC)_2]$

	THF exchanged MOF **(T1)**	*In situ* heating experiment 1 on THF exchanged MOF **(T2.5)**	*In situ* heating experiment 2 on THF exchanged MOF **(T3.3)**
Crystal Habit	Octahedron	Octahedron	Octahedron
Crystal Colour	Brown	Brown	Brown
Crystal Size (mm)	0.175 × 0.10 × 0.09	0.30 × 0.28 × 0.20	0.20 × 0.20 × 0.20
Crystal System	Orthorhombic	Orthorhombic	Orthorhombic
Space Group, Z	*Fddd*, 16	*Fddd*, 16	*Fddd*, 16
a (Å)	15.143(5)	15.201(3)	15.0952(4)
b (Å)	26.739(9)	27.482(6)	26.7260(7)
c (Å)	31.447(11)	30.868(6)	31.5195(8)
α (°)	90	90	90
β (°)	90	90	90
γ (°)	90	90	90
V (Å^3)	12733(7)	12895(4)	12716.0(6)
Radiation	Cu-K_α (λ = 1.54178 Å)	Cu-K_α (λ = 1.54178 Å)	Cu-K_α (λ = 1.54178 Å)
Density (g cm^{-3})[b]	1.084	1.070	1.085
Temperature (K)	100	298	298
μ (mm^{-1})[c]	6.230	6.107	6.239
2θ Range (°)	7.28 to 134.44	7.24 to 133.92	7.28 to 144.18
Reflns collected	16149	12627	28143
Independent reflns (R_{int})	2833 (0.0437)	2865 (0.0344)	3126 (0.0419)
Reflns used in refinement, *n*	2833	2865	3126
L.S. parameters, *p*	143	119	119
No. of restraints, *r*	0	4	0
Completeness	0.988	0.991	0.991
$R1(F)$[a] $I > 2\sigma(I)$	0.0674	0.0841	0.0666
$wR2(F^2)$[a], all data	0.2267	0.2705	0.2388
$S(F^2)$[a], all data	1.148	1.219	1.173

[a] $R1(F) = \sum(|F_o| - |F_c|)/\sum|F_o|$; $wR2(F^2) = \sqrt{\sum w\left(F_o^2 - F_c^2\right)^2/\sum wF_o^4}$; $S(F^2) = \sqrt{\sum w\left(F_o^2 - F_c^2\right)^2/(n+r-p)}$.

[b] Densities are calculated using only framework atoms and cations, and do not include guest molecules.

[c] Adsorption coefficients are calculated based on the crystallographic model

SQUEEZE analysis

The electron count in the pore was calculated using the routine SQUEEZE[23] in the program PLATON.[22] following the procedure detailed in section 3.3.3. The number of electrons per cell corresponds to both solvent and cations, with the number of electrons due to solvent being determined by subtracting the number of electrons associated with the cation and dividing by the number of formula units within one unit cell.

Table 7 – Electron count from SQUEEZE analysis of THF-exchanged MOF $(Me_2NH_2)[In(ABDC)_2]$

	Electrons per unit cell (in void spaces)	Solvent accessible void per unit cell ($Å^3$)	Electrons per Indium due to solvent [a]
T1	1664	7186.1	77
T2.5	395	7009.7	-2
T3.3	1141	6889.1	44

[a] Calculated by dividing the electron count per cell by Z and subtracting the electrons associated with the cations

3.3.6 Crystallographic studies of $CHCl_3$-exchanged $(Me_2NH_2)[In(ABDC)_2]$

In situ heating experiments

Crystals used for *in situ* heating were selected while immersed in $CHCl_3$, and one face of the crystal was glued to a glass fibre while the crystal was still covered in a thin layer of residual solvent. Care was taken to avoid coating the entire crystal in adhesive. The crystal was rapidly transferred to the diffractometer and situated in the nitrogen stream of the Cryostream device at room temperature. The glue was left to dry for 15 mins before any data were collected. Heating was carried out *in situ* using the Cryostream device. Two different heating experiments were carried out on two separate crystals (**T2** and **T3**). A ramp rate of 4 °C/min was used to raise the temperature, which was held at the final value for a fixed period (see Table 8) before cooling at a ramp rate of 4 °C/min. Measurements during the experiment were recorded at 298K, using the Cryostream to maintain the temperature. Full data collections were recorded for each point (**C1.1-3**). Table 8 details the heating study carried out and the resulting cell parameters. Full details of the crystallographic parameters are shown in Table 10. Figure 6 shows the behaviour compared to the observed single crystal breathing trend of the as-synthesised framework (**1-10** in chapter 2).

Table 8 - Parameters used and unit cell determined for crystallographic studies of desolvation by in situ heating

Temp heated	Hold time	Data Set Code	*a* (Å)	*b* (Å)	*c* (Å)	*V* (Å^3)
25 °C	Start	**C1.1**	15.4336(7)	27.6137(12)	30.6740(14)	13072.6(10)
150 °C	5 mins	**C1.2**	15.0441(6)	26.821(1)	31.4116(12)	12674.5(8)
150 °C	15 mins	**C1.3**	15.0597(5)	26.9731(9)	31.234(1)	12687.4(7)

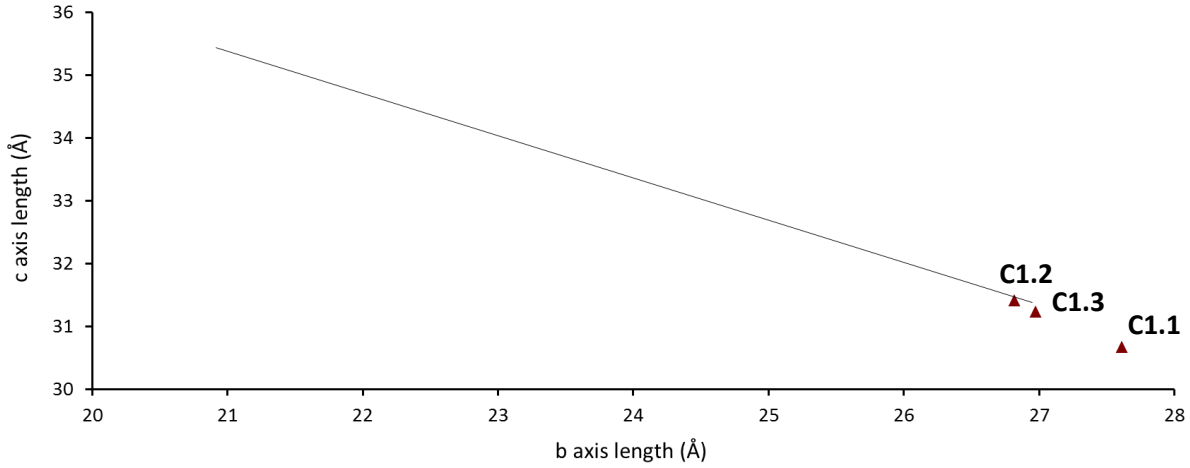

Figure 6 - Results of *in situ* heating experiment on $CHCl_3$ exchanged $(Me_2NH_2)[In(ABDC)_2]$ (**C1.1-1.3**) in comparison to the trend from single crystal desolvation studies of as-synthesised $(Me_2NH_2)[In(ABDC)_2]$ (**1-10**)

Ex situ drying in air

Crystals of $CHCl_3$-exchanged $(Me_2NH_2)[In(ABDC)_2]$ were transferred from the $CHCl_3$ solvent to a microscope slide and left for 6 hours to dry in air. A single crystal was mounted in a gas cell at beamline I19 (Diamond Light Source),[19] using Araldite adhesive to attach the crystal to a MiTeGen 50 µm MicroLoop, but was left under ambient conditions. X-Ray diffraction data were recorded at RT using synchrotron radiation as detailed in section 3.3.3. The crystal retained some crystallinity but the diffraction spots were visibly smeared on the detector images. The data were able to be integrated using a monoclinic cell, and the solved in space group *C*2/*c*, but with a low completeness. The unique indium atoms were able to be modelled anisotropically but all other framework atoms were modelled isotropically. The structure showed a phase change from the normal *Fddd* framework due to incorporation of water molecules. The crystallographic parameters are listed in Table 10.

SQUEEZE analysis

The electron count in the pore was calculated using the routine SQUEEZE[23] in the program PLATON.[22] following the procedure detailed in section 3.3.3. The number of electrons per cell corresponds to both solvent and cations, with the number of electrons due to solvent being determined by subtracting the number of electrons associated with the cation and dividing by the number of formula units within one unit cell.

Table 9 – Electron count from SQUEEZE analysis of $CHCl_3$-exchanged MOF $(Me_2NH_2)[In(ABDC)_2]$

	Electrons per unit cell (in void spaces)	Solvent accessible void per unit cell (Å^3)	Electrons per Indium due to solvent [a]
C1.1	2433	7243.0	125
C1.2	1749	6729.8	82
C1.3	1808	6589.4	86
C2	166	1788.3	-6

[a] Calculated by dividing the electron count per cell by Z and subtracting the electrons associated with the cations

Table 10 - Data collection, structure solution and refinement parameters single crystal X-ray structure determination of $CHCl_3$-exchanged MOF $(Me_2NH_2)[In(ABDC)_2]$

	In situ heating experiment on $CHCl_3$-exchanged MOF - 1 **(C1.1)**	*In situ* heating experiment on $CHCl_3$-exchanged MOF - 1 **(C1.2)**	*In situ* heating experiment on $CHCl_3$-exchanged MOF - 1 **(C1.3)**	$CHCl_3$-exchanged MOF dried in air **(C2)**
Crystal Habit	Octahedron	Octahedron	Octahedron	Octahedron
Crystal Colour	Brown	Brown	Brown	Brown
Crystal Size (mm)	0.30 × 0.30 × 0.30	0.30 × 0.30 × 0.30	0.30 × 0.30 × 0.30	0.26 × 0.26 × 0.17
Crystal System	Orthorhombic	Orthorhombic	Orthorhombic	Monoclinic
Space Group, Z	*Fddd*, 16	*Fddd*, 16	*Fddd*, 16	*C*2/*c*, 8
a (Å)	15.4336(7)	15.0441(6)	15.0597(5)	10.940(2)
b (Å)	27.6137(12)	26.821(1)	26.9731(9)	30.975(8)
c (Å)	30.6740(14)	31.4116(12)	31.234(1)	14.986(4)
α (°)	90	90	90	90
β (°)	90	90	90	99.97(2)
γ (°)	90	90	90	90
V (Å^3)	13072.6(10)	12674.5(8)	12687.4(7)	5002(2)
Radiation	Cu-K_α (λ = 1.54178 Å)	Cu-K_α (λ = 1.54178 Å)	Cu-K_α (λ = 1.54178 Å)	Synchrotron (λ = 0.6889 Å)
Density (g cm^{-3})[b]	1.056	1.089	1.088	1.427
Temperature (K)	298	298	298	RT[d]
μ (mm^{-1})[c]	6.084	6.259	6.253	0.911
2θ Range (°)	7.16 to 134.14	7.3 to 133.78	7.3 to 133.82	3.88 to 36.5
Reflns collected	17754	14919	16014	4244
Independent reflns (R_{int})	2913 (0.0578)	2817 (0.0629)	2822 (0.0595)	1619 (0.0635)
Reflns used in refinement, *n*	2913	2817	2822	1619
L.S. parameters, *p*	118	131	131	88
No. of restraints, *r*	5	9	13	0
Completeness	0.993	0.993	0.994	0.823
$R1(F)$[a] $I > 2\sigma(I)$	0.0892	0.0960	0.0977	0.1787
$wR2(F^2)$[a], all data	0.2901	0.2989	0.3064	0.4652
$S(F^2)$[a], all data	1.115	1.095	1.085	1.080

[a] $R1(F) = \sum(|F_o| - |F_c|)/\sum|F_o|$; $wR2(F^2) = \sqrt{\sum w\left(F_o^2 - F_c^2\right)^2/\sum wF_o^4}$; $S(F^2) = \sqrt{\sum w\left(F_o^2 - F_c^2\right)^2/(n+r-p)}$.

[b] Densities are calculated using only framework atoms and cations, and do not include guest molecules.

[c] Adsorption coefficients are calculated based on the crystallographic model

[d] Exact temperature unknown, because no Cyrostream was used during the measurement

3.3.7 Bulk phase analysis of $CHCl_3$-exchanged $(Me_2NH_2)[In(ABDC)_2]$

Comparisons between different samples

Powdered samples were prepared by filtering single crystals of $CHCl_3$-exchanged $(Me_2NH_2)[In(ABDC)_2]$ under vacuum, and grinding in a pestle and mortar. X-Ray diffraction data were recorded for three different samples (**PC1-3**) either using synchrotron radiation at the I11 beamline[24] at Diamond Light Source (**PC1**) , λ = 0.82562(2) Å, or on the Bruker D8 Advance instrument using Cu-K_α radiation (**PC2** and **PC3**). All data was recorded at room temperature and 2θ values in Figure 7 have been scaled to the wavelength used for the synchrotron data collection. Significant variations are seen between the patterns due to differing relative compositions of two crystalline phases. The phases correspond to the $CHCl_3$-exchanged MOF **C1.1** and the dried-in air phase **C2**.

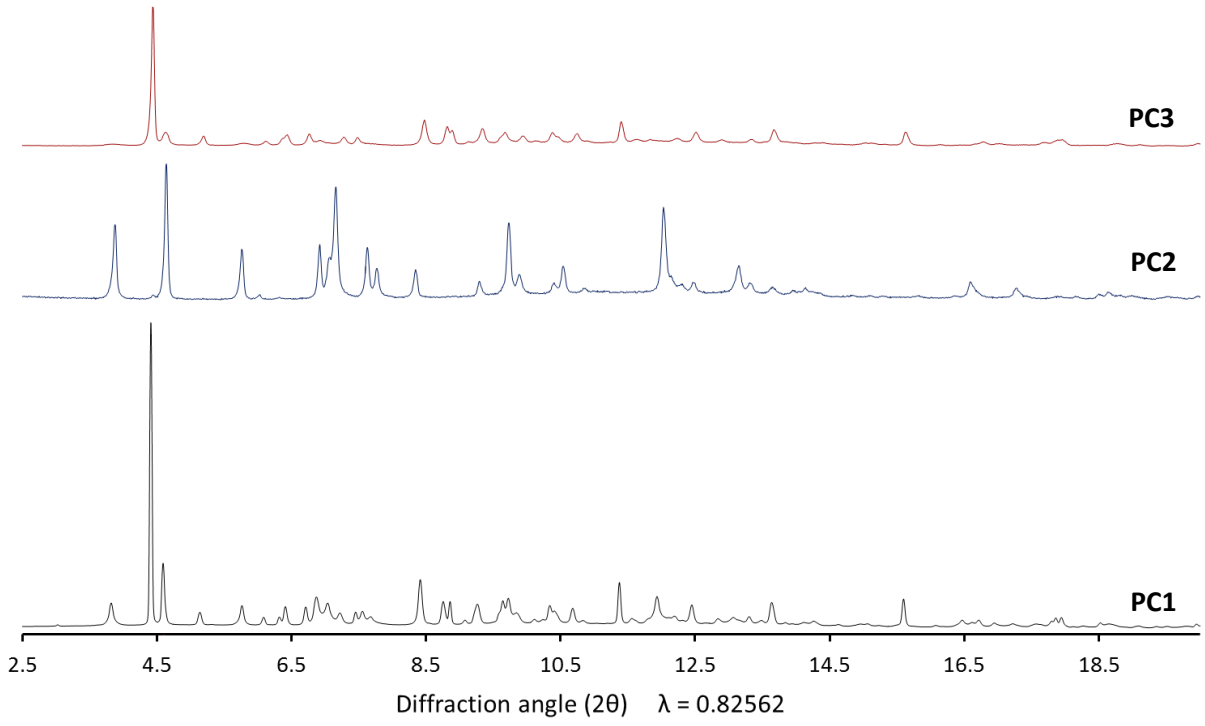

Figure 7 - X-ray powder diffraction patterns of 3 different $CHCl_3$-exchanged $[In(ABDC)_2Me_2NH_2]$ samples **PC1-3**. Patterns have been scaled in 2θ and represented using 2θ values corresponding to λ = 0.82562 Å.

Multi-phase Pawley fitting of **PC1**

The two-phase behaviour of **PC1** was confirmed using a two-phase Pawley refinement. The unit cell parameters of the two phases were determined by an indexing algorithm in TOPAS,[26] using carefully selected reflections known to correspond to only to one of the phases in each case. The two-phase Pawley refinement[28] employed 2,589 parameters (13 background, 1 sample displacement error, 8 profile, 7 cell and 2,560 reflections), resulting in final indices of fit R_{wp} = 4.398, $R_{wp'}$ = 9.377. The final unit cell parameters were orthorhombic a = 15.374 (2) Å, b = 27.378 (3) Å, c = 30.913 (3) Å, V = 13011 (2) Å and monoclinic a = 10.9751 (5) Å, b = 30.9557 (1) Å, c = 14.9696 (6) Å, β = 100.728 (4) °, V = 4996.9 (4) Å^3. The fit is displayed in Figure 8.

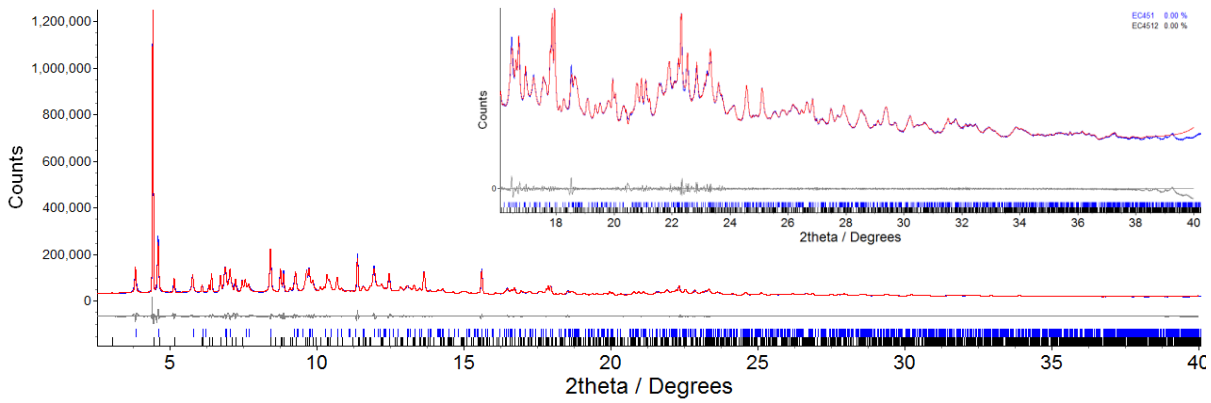

Figure 8 – Observed (blue) and calculated (red) and difference plot [I_{obs} - I_{calc}] (grey) of the two-phase Pawley[28] refinement of $CHCl_3$-exchanged $(Me_2NH_2)[In(ABDC)_2]$ (**PC1**) (2θ range 3.0 – 40.0 °, d_{min} = 1.2Å).

Rietveld refinement of **PC3**

The identity of the structure of sample **PC3** was confirmed through Rietveld refinements, which displayed the highest phase purity for phase **C2**. The unit cell parameters and framework atoms of single crystal structure **C2** were used as a starting point for a single-phase Rietveld[31] refinement employing 27 parameters (14 background, 1 zero error, 5 profile, 4 cell, 1 scale and 2 occupancy), resulting in final indices of fit R_{wp} = 10.833, $R_{wp'}$ = 28.343. The final unit cell parameters were monoclinic a = 10.934 (1) Å, b = 30.910 (5) Å, c = 14.963 (2) Å, β = 100.369 (9) °, V = 4974 (1) Å^3. The positions and orientations of the cation and solvent molecules within the pore (modelled as rigid bodies) were optimised by simulated annealing. The fit is displayed in Figure 9; the unfitted peaks at 2θ 7.7, 8.7 & 10.8 ° indicate the presence of a small amount of phase **C1.1**, but an insufficient number of peaks were present for a reliable two phase Rietveld refinement.

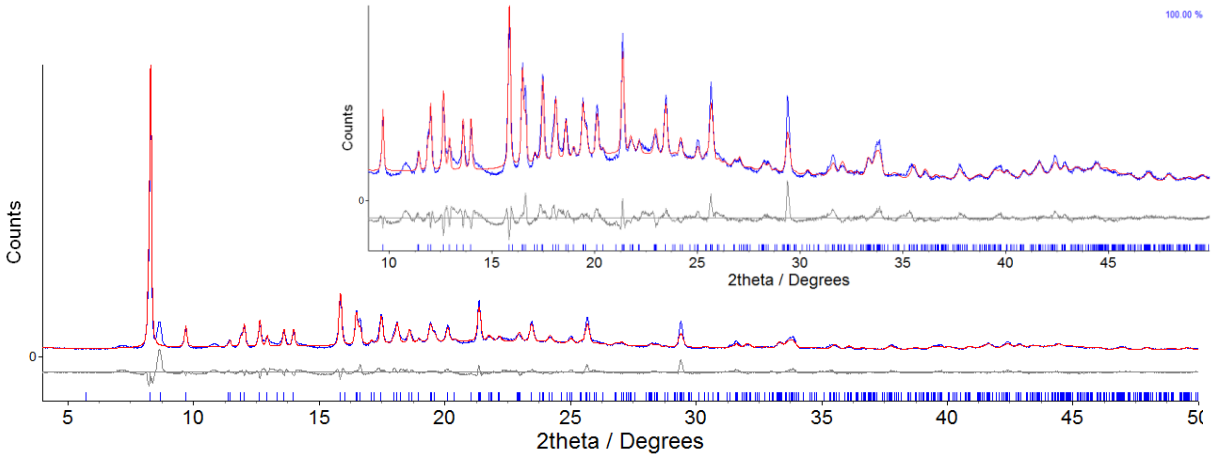

Figure 9 - Observed (blue) and calculated (red) and difference plot [I_{obs} - I_{calc}] (grey) of the Rietveld[31] refinement of $(Me_2NH_2)[In(ABDC)_2(H_2O)].1.73H_2O$ (**PC3**) (2θ range 4.0 – 50.0 °, d_{min} = 1.82Å).

In situ heating of multiphase pattern **PC1**

The powdered sample **PC1** was packed into a 0.7mm borosilicate capillary with one end cut open and mounted on the diffractometer at beamline I11[24] at Diamond Light Source, λ = 0.82562(2)Å. The nitrogen stream of the Cryostream device was positioned co-axial to the capillary and X-ray data were recorded at 298 K (**PC1.1**). The Cryostream was then ramped to 353 K (80 °C) at 6 °C / min and the sample was maintained at 80 °C for 20 mins before further X-ray data were collected (**PC1.2**). The process was repeated for heating to 373 K (100 °C) (**PC1.3**). The Cyrostream was then cooled to 300 K (27 °C) at 6 °C / min and a final powder pattern recorded (**PC1.4**). The powder patterns are plotted in Figure 10. The patterns show a clear reduction of peaks corresponding to **C2** (denoted by triangles) and a growth pf peaks corresponding to **C1.3** (asterisks)

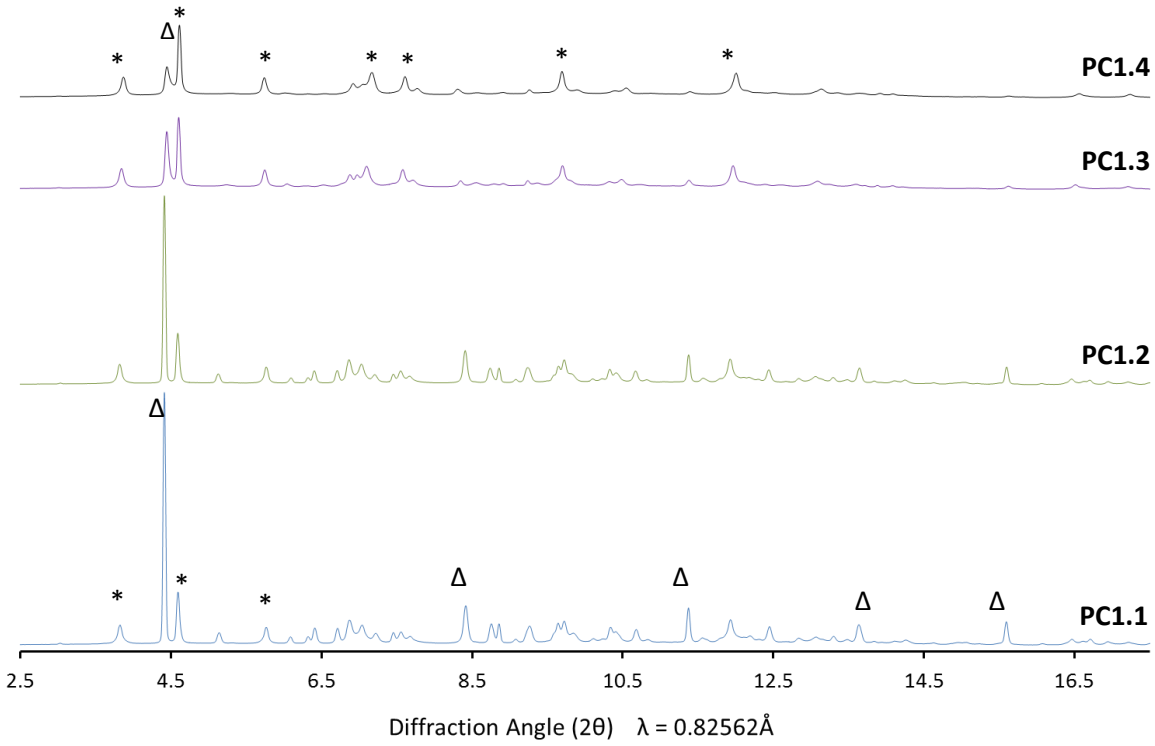

Figure 10 - *In situ* heating experiment on $CHCl_3$-exchanged $(Me_2NH_2)[In(ABDC)_2]$ (**PC1.1 to PC1.4)**. Asterisks and triangles correspond to peaks of **C1.3** and **C2** respectively.

Atmospheric water uptake

A powdered sample of $CHCl_3$-exchanged MOF $(Me_2NH_2)[In(ABDC)_2]$ was heated at 80 ^oC under constant nitrogen flow for 1 hour within a Schlenk tube. The sample was then transferred to an argon-filled glovebox and packed into a 0.7 mm borosilicate capillary. The capillary was flame-sealed immediately upon removal from the glovebox and X-ray data recorded on the Bruker D8 diffractometer using Cu-K_α radiation (**PC4.1**). The end of the capillary was then cut open and left exposed to air for 48 hrs to permit atmospheric water uptake before the powder pattern was re-collected (**PC4.2**). The powder patterns are displayed in Figure 11, showing a conversion from **C1.3** towards **C2**. The peaks corresponding to **C1.3** and **C2** are denoted by asterisks and triangles respectively.

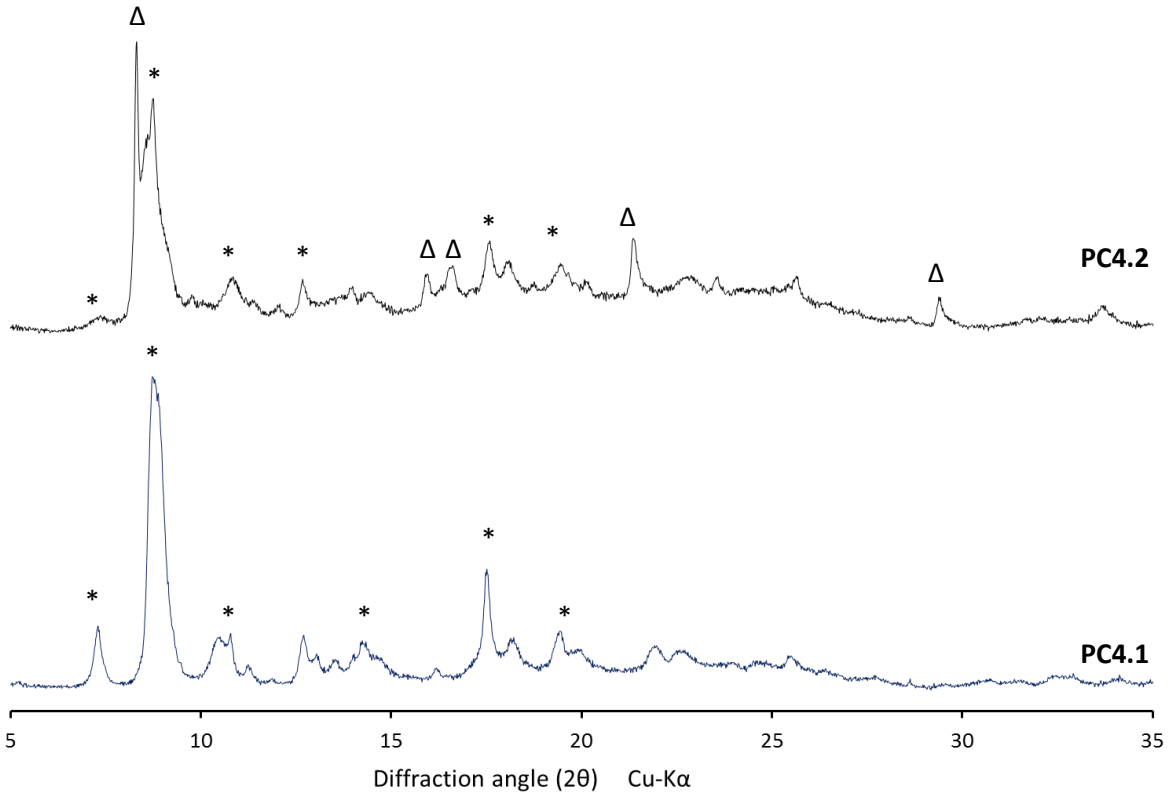

Figure 11 - Atmospheric water uptake experiment on $CHCl_3$-removed $(Me_2NH_2)[In(ABDC)_2]$ (**PC4**)

3.3.8 Complementary techniques for $[In(ABDC)_2Me_2NH_2].CHCl_3$

NMR spectroscopy

A solution-phase ^1H NMR spectrum of the framework after solvent exchange was obtained after following the digestion method described in Section 3.3.3 (Figure 12). Integration of the proton environments suggests 0.75 $CHCl_3$ molecules per indium. An expanded section between 7.1 – 8.5ppm is shown in Figure 13

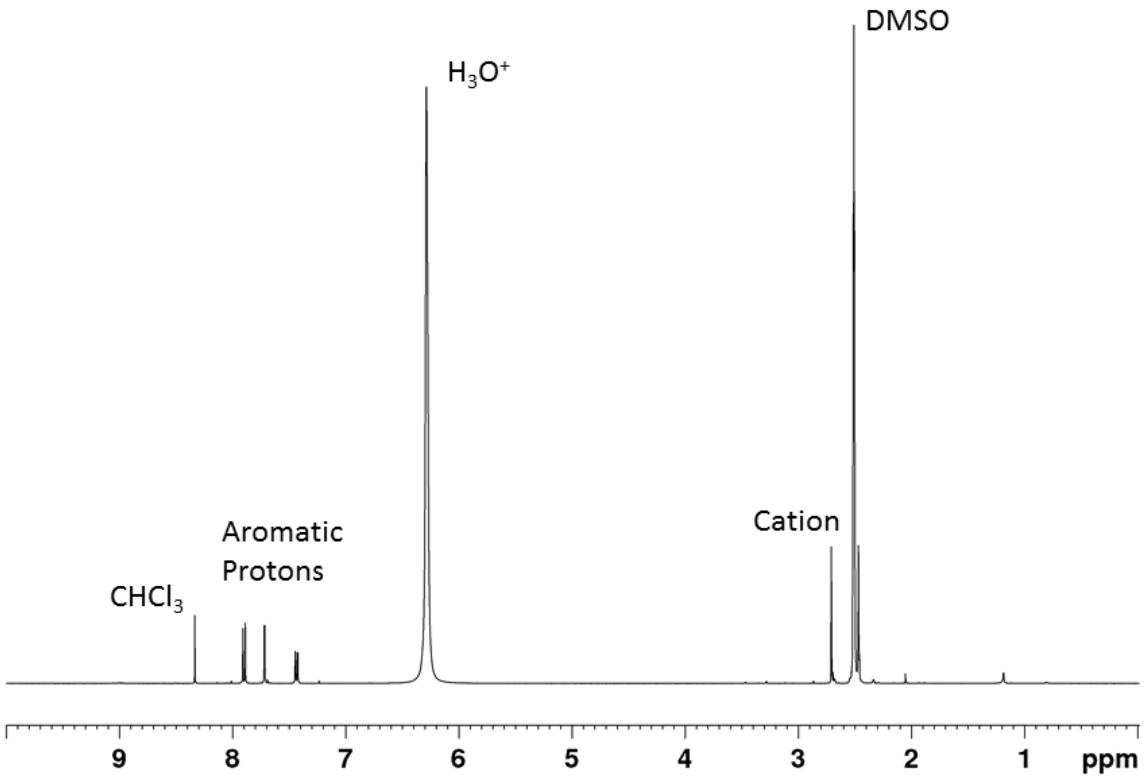

Figure 12 – Solution phase ^1H NMR spectrum of $CHCl_3$ exchanged MOF $(Me_2NH_2)[In(ABDC)_2]$ after digestion

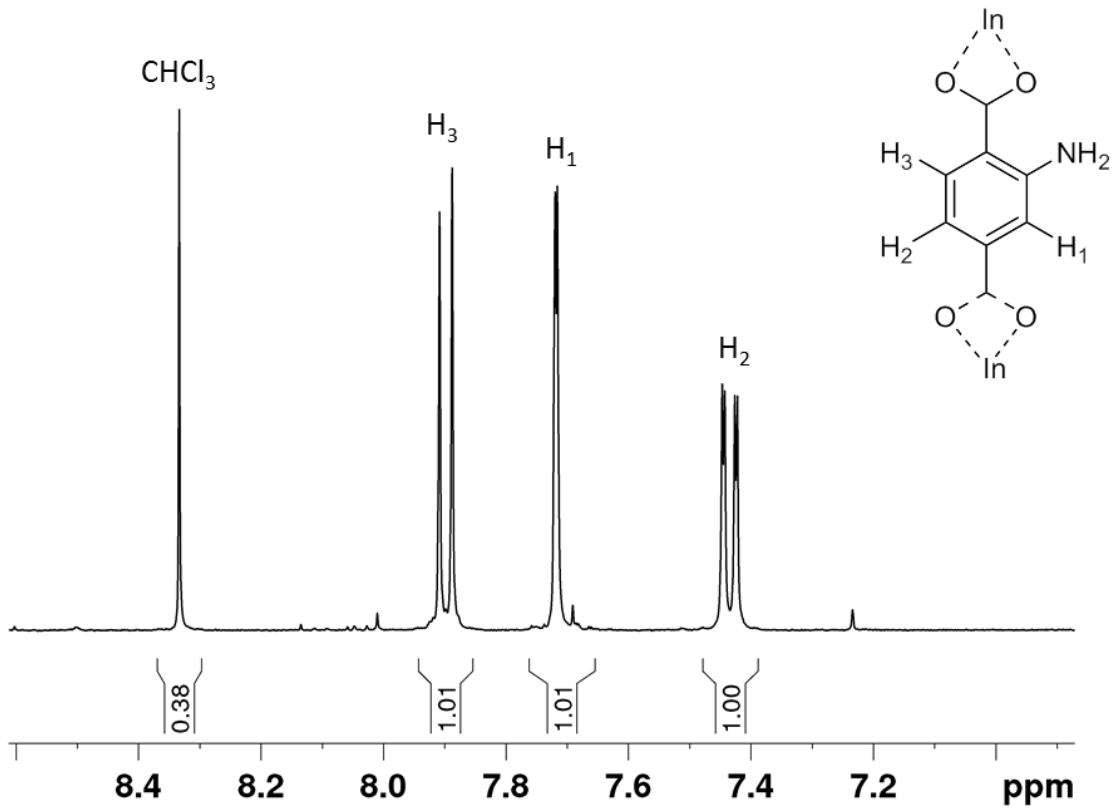

Figure 13 – Expanded range of the solution phase ^{1}H NMR spectrum of $CHCl_3$ exchanged MOF $(Me_2NH_2)[In(ABDC)_2]$ after digestion

Thermogravimetric analysis

The thermal decomposition of the $CHCl_3$-exchanged frameworks under a nitrogen atmosphere was followed using TGA analysis. An example trace is shown in Figure 14 and contains 4 distinct steps, the first one while holding at 25 °C, the second between 60 °C and 100 °C, the third at about 250 °C, and the final step at 400 °C.

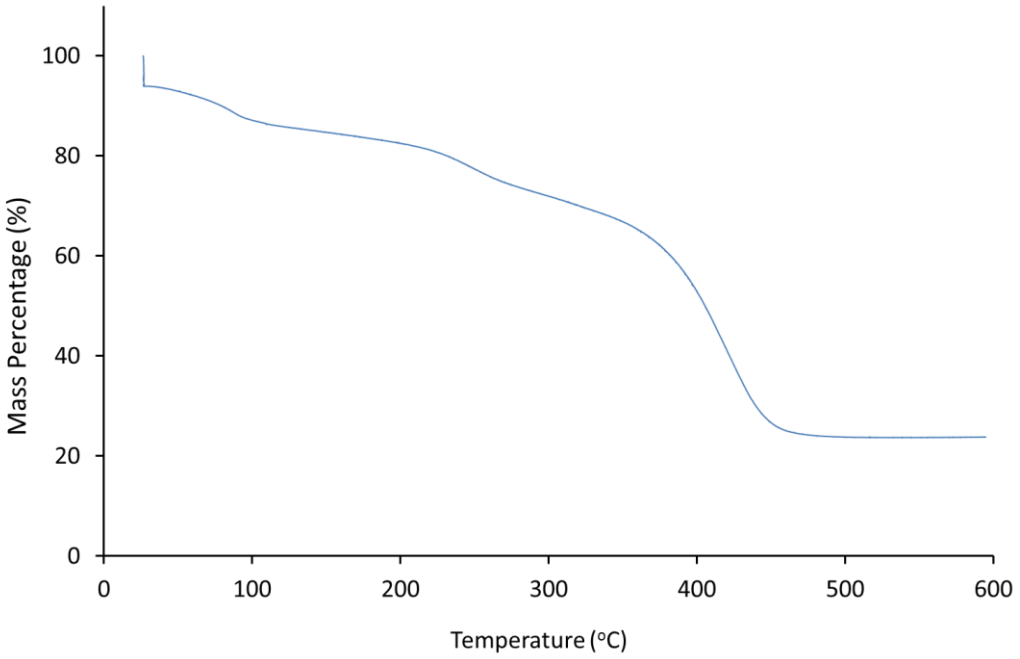

Figure 14 - Thermogravimetric analysis of $CHCl_3$-exchanged $(Me_2NH_2)[In(ABDC)_2]$ between 25 °C and 600 °C, The temperature was held at 25 °C for 30 mins before ramping at 4 °C/min

3.4 Results and Discussion

3.4.1 Solvent exchange with acetone

Single crystal structures

After solvent exchange, based on literature methods,[5, 7] the single crystals of the MOF remained intact, allowing accurate structural characterisation by X-ray diffraction. Five full data sets (**A1-5**) were collected, and refinements of the structures suggest that the framework maintains the same overall topology. The structures exhibit a partial closing of the pore along the known breathing trend line of the as-synthesised framework, despite being solvated and not exposed to air. This effect can be seen in Figure 15 which plots the *b* and *c* unit cell axis values for the acetone-exchanged crystals (**A1-5**) in comparison to the trend line from crystals **1-10**. The degree of pore opening between the different crystal structures is variable and correlates reasonably well to the number of electrons determined from SQUEEZE analysis. This indicates flexibility in the framework similar to the as-synthesised material, occurring due to differing solvent content.

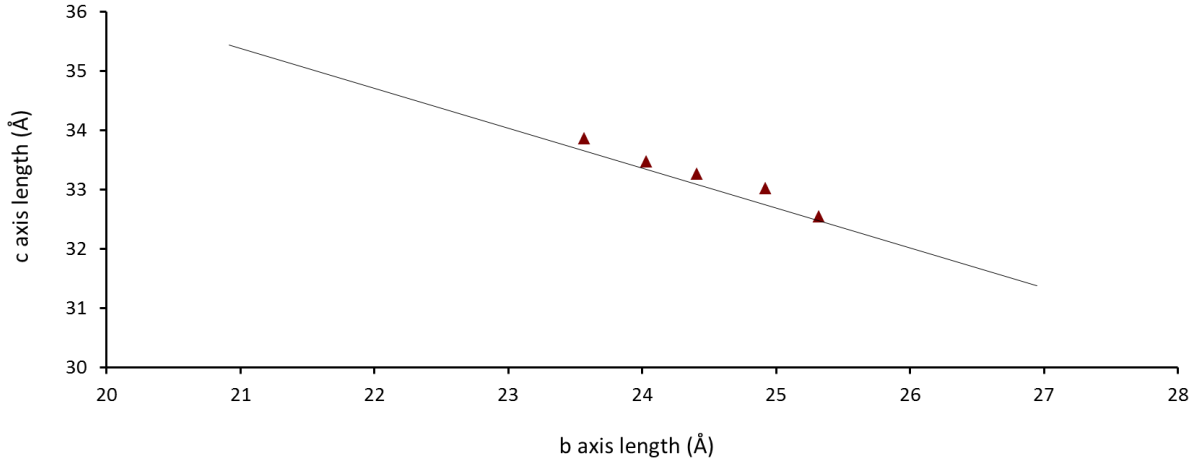

Figure 15 – *b* and *c*- axis values of acetone-exchanged $(Me_2NH_2)[In(ABDC)_2]$ (**A1-5**) in comparison to the trend line from single crystal desolvation studies of as-synthesised $(Me_2NH_2)[In(ABDC)_2]$ (**1-10**). All data were recorded at 100K

The crystal structures of the acetone-exchanged framework (**A1-5**) do not exhibit suitable systematic absences for the expected *Fddd* space group, and the presence of satellite reflections suggest a modulated structure. The refinements of the crystal structure in space group *Fddd* suggest high electron density peaks (5 $e^-/Å^3$) contained within the pore, which can't be suitably modelled as cations or guest molecules. Failure to account for these features in the model results in high R1 and

wR2 values. The R factor is reduced if the electron density from the disordered solvent, leading to diffuse electron density, is modelled with the SQUEEZE routine within the program PLATON.[23] One possibility is that an ordering of the pore contents occurs with a different periodicity to the framework structure, *i.e.* modulation, and gives rise to the satellite reflections. This may prevent the cations and solvent molecules being modelled appropriately unless the modulation can also be modelled. Similar results have previously been reported in IM-19 [Ga(OH)(BDC)], a gallium analogue of the flexible MOF MIL-53, which also showed satellite reflections in the precession reconstruction of the post-synthesis material.[32] The additional reflections were able to be described using an incommensurate q-vector and were attributed to a sub-lattice of ordered guest BDC ligands believed to strongly interact with the framework. The BDC ligands could be seen in the Fourier map but a full description of the guest ligands using the superspace group formalism wasn't presented.[32] To the authors knowledge no subsequent follow up papers have been since been published.

Solvent Removal

The removal of the solvent was probed by two crystallographic *in situ* heating experiments (**A6** and **A7**). The studies allowed the desolvation of the framework to be observed in the absence of water uptake. The results show highly closed pore structures, either directly upon mounting in the Cryostream at room temperature (**A7.1**) or after heating at only 60-80 ^{o}C (**A6.2**-**4**). These observations resemble those obtained by DMF removal during *in situ* heating experiments on the as-synthesised MOF (**H1.6** & **H2.2**), albeit at higher temperatures. The changes to the *b*- and *c*-axes during *in situ* heating experiment **A6** are shown in Figure 16, revealing good agreement with the previously observed trend line. The SQUEEZE analysis of residual electron density in the solvent accessible voids of **A6.4** showed a reduction in the electron count compared to the solvent exchanged frameworks, but not a total removal of solvent. The diffraction data displayed the correct systematic absences for space group *Fddd*, little evidence of satellite peaks in the precession images, and the crystal structure was able to be solved to a reasonable R1 value without the use of SQUEEZE to model the disordered cations and any residual solvent content in the pores.[23] This suggests a removal of the acetone molecules removes the potential modulation effects described for **A1-5**.

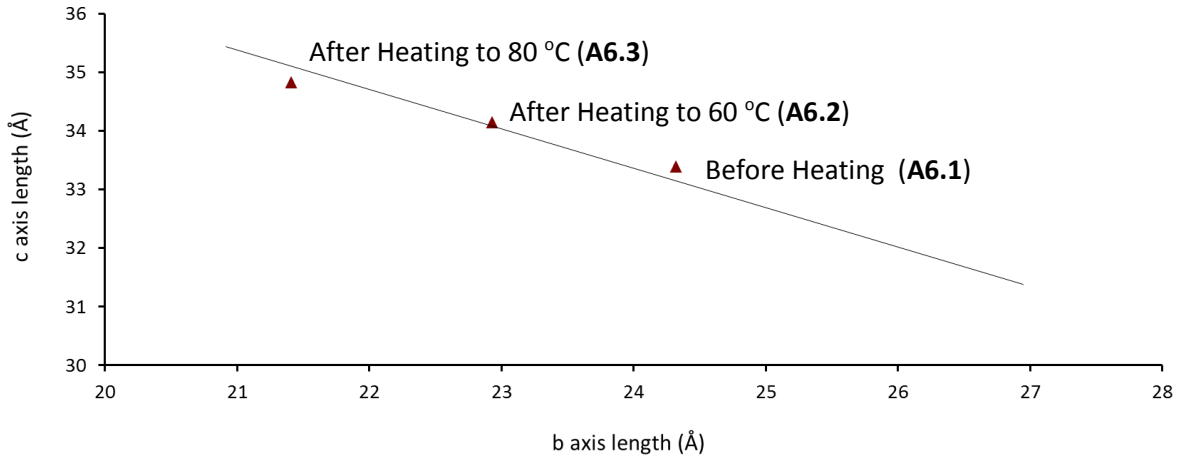

Figure 16 - Results of *in situ* heating experiment **A6** on acetone-exchanged $(Me_2NH_2)[In(ABDC)_2]$ (**A6.1-6.4**) in comparison to the trend line from single crystal desolvation studies of as-synthesised $(Me_2NH_2)[In(ABDC)_2]$ (**1-10**). **A6.1-3** were recorded at 298K, **A6.4** was recorded at 298K

3.4.2 Solvent exchange with THF

The single crystal structure of the THF-exchanged framework (**T1**) did not any show movement along the known trend line for the flexible behaviour of the MOF and exhibited an open pore structure very similar to the as-synthesised material. This suggests little or no solvent loss prior to data collection. A small pore contraction occurs consistent with the low temperature (100 K) data collection, as observed for low temperature studies in Chapter 2. Two *in situ* heating experiments were carried out to observe the effects of desolvation (**T2** and **T3**). Interestingly, these experiments show that the framework remains in an open-pore form, suggesting that contrary to both the DMF and acetone-containing versions of the MOF, the THF-exchanged crystals do not exhibit the large breathing effect. The two end points of the *in situ* heating experiments (**T2.5** and **T3.3**) are shown in Figure 17 and compared to known breathing trend line of the as-synthesised framework. Crystal structure **T2.5** is of particular relevance, as SQUEEZE analysis suggests it has been fully desolvated. The MOF therefore shows a solvent dependence in its flexibility and is stable in an open desolvated form.

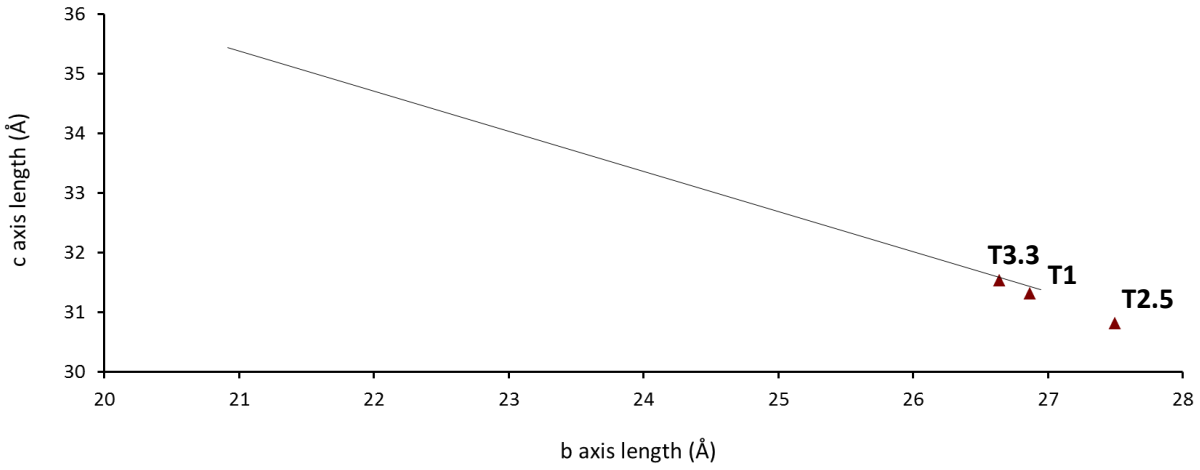

Figure 17 – *b*- and *c*-axis values of THF-exchanged $(Me_2NH_2)[In(ABDC)_2]$ **T2.5** & **T3.3** in comparison to the trendline from single crystal desolvation studies of as-synthesised $(Me_2NH_2)[In(ABDC)_2]$ (**1-10**). **T1** was recorded at 100K. **T2.5** and **T3.3** were recorded at 298K

3.4.3 Solvent exchange with $CHCl_3$

In situ heating experiments

The solvent dependence of $(Me_2NH_2)[In(ABDC)_2]$ was further probed by an *in situ* heating experiment on a $CHCl_3$-exchanged framework (**C1**), with full data sets collected and structure determinations undertaken after each heating step (**C1.1** - **1.3**). The structure showed very similar behaviour to the THF-containing version, remaining mostly in an open-pore form. This correlates well with the original literature report in which a $CHCl_3$-exchanged framework was desolvated prior to volumetric gas uptake measurements, and showed the powder diffraction pattern of the framework closely resembled that of the as-synthesised open framework. The result suggests two possible paths during desolvation; a large continuous closing mechanism, or a more rigid behaviour, with the framework staying in the open-pore form with only a small degree of motion. The difference in the behaviour appears to lie in the polarity of the solvents; $CHCl_3$ and THF are less polar than DMF and acetone, and therefore are likely to interact less strongly with the framework or the cations contained within the pores. Removal of solvent in the DMF- or acetone-containing materials causes the framework to close around the remaining solvent molecules to maintain the same framework-guest interactions. A continuum of structures is then created by a constantly changing solvent content. The framework-guest interactions are much weaker in the $CHCl_3$- and THF-exchanged MOFs, and therefore the framework does not show the large dynamic motion on solvent removal. A schematic for the behaviour of the MOF on removal of $CHCl_3$ compared to removal of DMF is displayed in Figure 18.

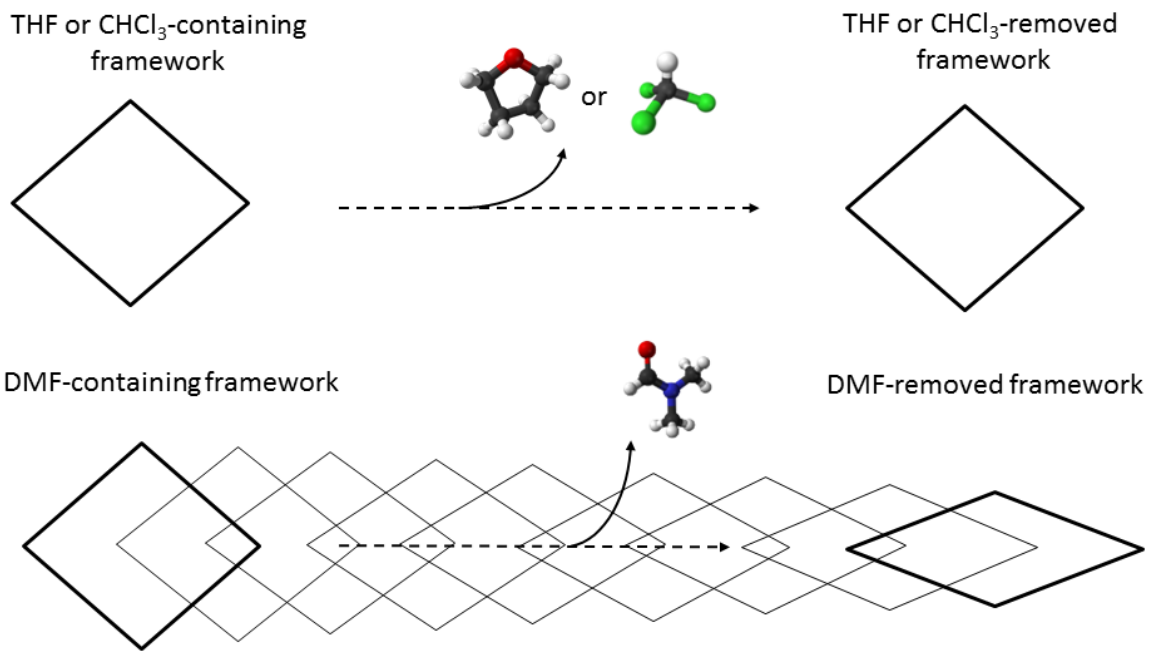

Figure 18 – Exaggerated schematic showing the pore shape changes of the $(Me_2NH_2)[In(ABDC)_2]$ upon loss of either $CHCl_3$ or DMF guests

The structure of the fully desolvated framework obtained from DMF or acetone removal has not been crystallographically characterised and therefore is not known. This presents two possibilities. The first is that the pores only remain closed due to an interaction with the small amount of remaining solvent, and complete desolvation would result in a return to the open framework, this would show parallels to other flexible frameworks such as MIL-53.[33–35] The second is that the solvent dependence results in two different desolvated frameworks, an open-pore form and a closed-pore form, requiring two thermodynamic minima. The latter is a very uncommon behaviour but not unprecedented. The MOFs MIL-69[36] and DUT-4[37] (Figure 19) are two different forms of the same MOF, with framework formula [Al(OH)(ndc)], ndc = naphthalene-2,6-dicarboxylate. Synthesised solvothermally from water and DMF solvent, respectively, the two frameworks exhibit the same connectivity, but the MIL-69 exists in a narrow-pore form both when solvated and desolvated, and DUT-4 exists in a large-pore form as both the solvated and desolvated material. Both are reported to be rigid-framework materials and all attempts to interconvert the two forms have been unsuccessful.[37, 38] The consequences of $(Me_2NH_2)[In(ABDC)_2]$ being able to exist in desolvated open-pore and closed-pore forms will be explored in further depth in chapter 4.

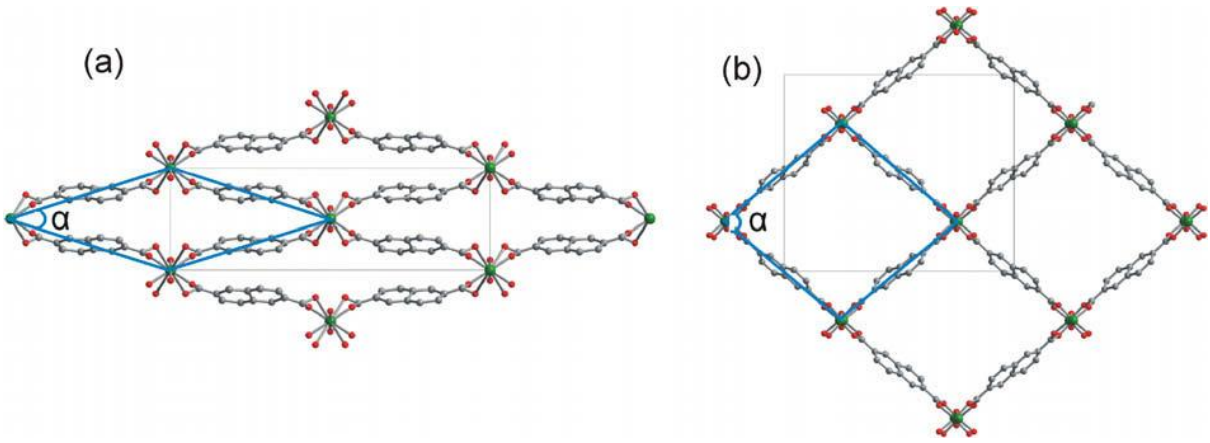

Figure 19 - Structural representations of a) MIL-69 and b) DUT-4. Reprinted with permission from I. Senkovska *et al*., *Microporous Mesoporous Mater.*, 2009, 122, 93–98. Copyright 2009 Elsevier.[37]

Exposure to air

Removing the $CHCl_3$-exchanged MOF from the $CHCl_3$ solvent and exposing it the air for 6 hours was found to result in a defined phase transition (structure **C2**). This behaviour is different from that of the as-synthesised framework which was observed to close instead (structures **4** and **5**). The phase change occurs because of coordination of two water molecules to half of the indium atoms. This gives rise to two crystallographically independent indium atoms, which results in a change in crystallographic symmetry from orthorhombic *Fddd* to monoclinic *C*2/*c.* One of indium atoms displays the previously observed flattened tetrahedral geometry, caused by the 4 chelating carboxylic acid groups, while the other is coordinated by 4 monodentate carboxylate groups and two water molecules in an octahedral arrangement. Similar coordination changes to metal centres in extended framework materials during the loss or gain of water molecules are well known. Examples include $[Cu(CPNA)(Me_2NH)].H_2O$ (H_3CPNA = 5-(4'-carboxylphenoxy)nicotinic acid) which shows a SC-SC transition from a four coordinated Cu environment to a five coordinated Cu environment when soaked in CH_2Cl_2,[39] $[Co(Hoba)_2 2H_2O]$ (H_2oba = 4,4'-oxybis(benzoic acid)) undergoing a octahedral to tetrahedral change during removal of its 2 coordinated water molecules by heating,[40] and $[Zn_2(tp)_2(DFPB)]$ (H_2tp = terephthanlic acid, DFPB = 2,3-difluoro-1,4-bis(4-pyridyl)benzene) displaying the coordination of water to a deformed paddlewheel node upon exposure of the activated material to air.[41] These changes however usually occur to all of the framework's metal centres or SBUs at once, unlike the behaviour exhibited in **C2**. The two indium environments of **C2** are displayed in Figure 20. The structure is stabilized by hydrogen bonding between the hydrogens of the water molecule and carboxylate oxygens located on both the same network and the other interpenetrated chain.

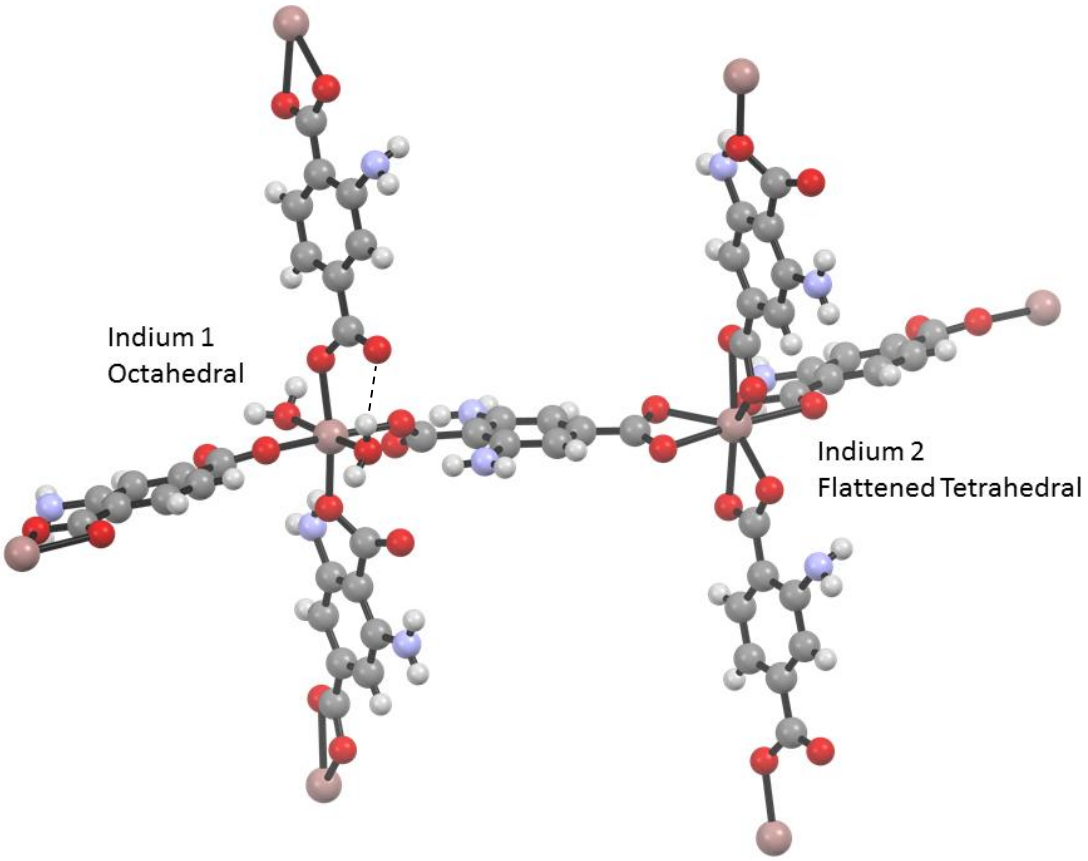

Figure 20 - Representation of $(Me_2NH_2)[In(ABDC)_2(OH_2)]$ displaying the two different indium environments. Cations and non-coordinated solvent molecules were not able to be resolved crystallographically. A hydrogen bonding interaction between the coordinated water and the carboxyl oxygen is shown in black at a distance of 2.05Å.

Solution-phase ^1H NMR analysis shows the air-dried MOF contains only 0.75 $CHCl_3$ molecules per indium, which is low considering the as-synthesised framework contains approximately 2 DMF molecules. The framework therefore is suspected to have lost a reasonable amount of $CHCl_3$, and replaced it with water absorbed from the air. The crystallographic model for the new phase could not be refined anisotropically, but the isotropic displacement parameters refined to reasonable values, and the oxygen atoms of the water molecules were clearly evident in the residual electron density.

The geometrical changes caused by conversion of half of the indium centres to the octahedral environment results in a tighter coiling of the helical chains running along the pore direction, coupled with a slight distortion of the pore shape. This gives a pore volume reduction of 50%, which is greater than during the breathing effect of the as-synthesised framework (**1** *vs* **9** is a 31% change). The main movement can be considered to be like the compression of a spring, and is displayed in Figure 21.

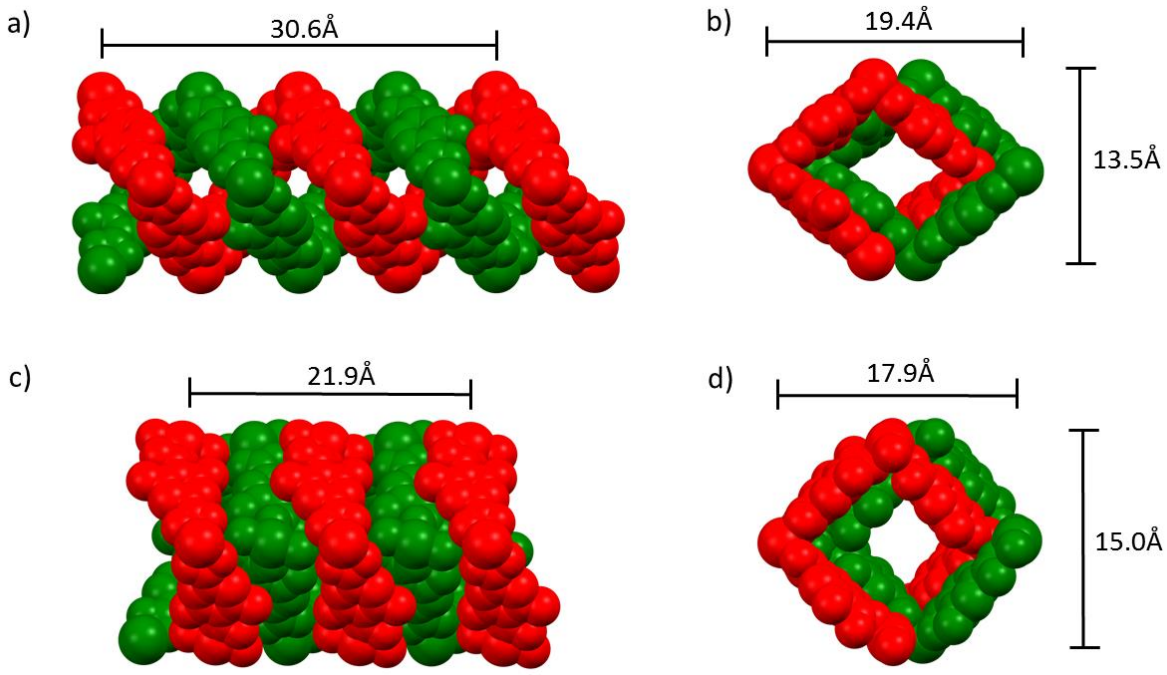

Figure 21 – Space-filling representation of the differences between the open-pore structure of a) - b) $(Me_2NH_2)[In(ABDC)_2]$ (**1**) and c) - d) the water bound MOF$(Me_2NH_2)[In(ABDC)_2(OH_2)]$ (**C2**). a) and c) show the two interpenetrated helical chains viewed along the *c*-axis with the *a*-axis horizontal and *b*-axis vertical, and b) and d) show the channel shape viewed down the *a*-axis with the *b*-axis horizontal and *c*-axis vertical.

No evidence of a phase with water molecules coordinated to all indium centres has been observed. This is suspected to be due to steric constraints. The change of half the indium centres to an octahedral coordination environment causes a closer packing of the interpenetrated chains leaving insufficient space for bound water molecules on neighbouring indium atoms.

3.4.4 Bulk phase analysis of $CHCl_3$-exchanged $(Me_2NH_2)[In(ABDC)_2]$

Variations between different samples

The effect of the $CHCl_3$ exchange on the bulk sample (rather than individual single crystals) was examined using X-ray powder diffraction. Diffraction patterns for three different $CHCl_3$-exchanged samples were recorded (**PC1-3**). These patterns are significantly different to each other, due to different ratios of the two known crystalline phases, open-pore $(Me_2NH_2)[In(ABDC)_2]$ and water-coordinated $(Me_2NH_2)[In(ABDC)_2(OH_2)]$. **PC1** showed a roughly equal mixture of the two phases, **PC2**

almost phase pure open-pore MOF, and **PC3** was close to being phase-pure for the water-coordinated $(Me_2NH_2)[In(ABDC)_2(OH_2)]$, with only a small amount of the open-pore $(Me_2NH_2)[In(ABDC)_2]$. Figure 22 shows the 3 patterns in comparison to the predicted patterns from the two single crystal structures. A two-phase Pawley[28] refinement of **PC1** resulted in unit cell parameters for the two phases similar to those of open-pore $(Me_2NH_2)[In(ABDC)_2]$ (**C1.1**) and $(Me_2NH_2)[In(ABDC)_2(OH_2)]$ (**C2**). A Rietveld[31] refinement of **PC3** using the structure **C2** as a starting point showed a good match to the experimental data.

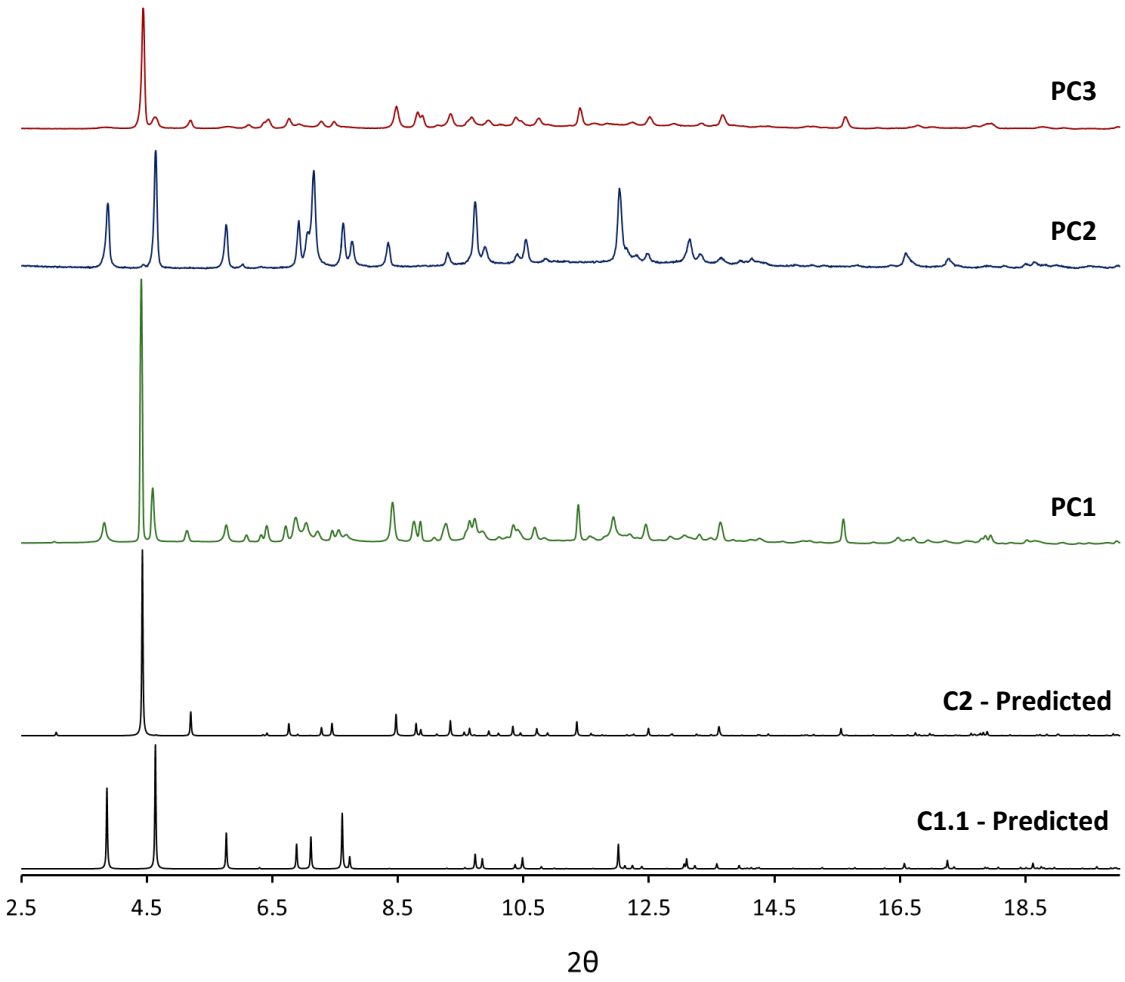

Figure 22 - Powder diffraction patterns of $CHCl_3$-exchanged $(Me_2NH_2)[In(ABDC)_2]$ **PC1-3** in comparison to predicted powder patterns of single crystals **C1.1** and **C2**.

In situ heating and atmospheric water uptake experiments

An *in situ* heating experiment on **PC1** was carried out to observe the effects of desolvation on the mixed-phase material. The patterns (**PC1.1-1.4**) showed a conversion towards phase-pure open-pore MOF $(Me_2NH_2)[In(ABDC)_2]$ upon heating, and further progression upon increased heating. This suggests loss of the coordinated water molecules and a return towards a flattened tetrahedral connectivity at all indium centres. During the experiment no evidence of pore closing was observed, therefore desolvation of $(Me_2NH_2)[In(ABDC)_2(OH_2)]$ appears to result in an structure similar to the as-synthesised material. This is confirmed by the pattern measured after *ex situ* heating (**PC4.1**), which shows an essentially phase-pure open-pore framework after solvent removal by heating under nitrogen. The effect appears to be reversible with exposure of the desolvated open-pore material $(Me_2NH_2)[In(ABDC)_2]$ to atmospheric vapour leading to formation of the water-coordinated $(Me_2NH_2)[In(ABDC)_2(OH_2)]$, as indicated the mixed-phase powder pattern (**PC4.2**). This behaviour implies that the water uptake is different in the open empty framework compared to the partially desolvated as-synthesised framework (**W1.1**), which instead displayed a continual opening when taking up water upon exposure to air (see chapter 2). The behaviour is also significantly different to water adsorption in MIL-53(Cr) [Cr(OH)(BDC)], in which the desolvated MOF undergoes a large-pore to narrow-pore phase transition, forming hydrogen bonding interactions with the absorbed water molecules.[33] The difference in the behaviour to MIL-53 may relate to the fixed wine-rack framework topology of MIL-53 *vs* the diamondoid structure of the $(Me_2NH_2)[In(ABDC)_2]$; the higher freedom allowing the large changes to the geometry, but may also be due to differences in the ability to insert water into the different metal-carboxylate bonds.

3.5 Conclusions

This chapter has shown that the continuous breathing mechanism of $(Me_2NH_2)[In(ABDC)_2]$ described in chapter 2 is solvent-dependent. The framework containing the less polar solvents $CHCl_3$ and THF shows very limited dynamic motions during desolvation, but the framework containing the more polar solvents DMF and acetone displays large dynamic motions associated with pore opening/closing. The solvent-dependence is suspected to be due to the strength of the solvent-framework interactions and offers the potential of two different empty-pore structures, one open and one closed, which are likely to exhibit different behaviour during subsequent applications. Crystallographic studies of the acetone-exchanged framework have also revealed the possibility of a modulation in the crystal structure which is removed on loss of acetone, and therefore may be related to ordering of guest molecules with a different periodicity to the framework itself. Exposure of the $CHCl_3$-exchanged MOF to air shows further dynamic framework motions not exhibited by the as-synthesised MOF. Here the framework undergoes a defined phase transformation to a new phase in which two water molecules are bound to half of the indium atoms. The coordination of the water molecules changes the geometry around the metal centre, reducing the pore size and pore length, leading to a change in crystallographic symmetry and a significant decrease in volume. The presence of the new phase appears in the bulk $CHCl_3$-exchanged samples to differing extents but can be removed by heating to give the desolvated open-pore MOF.

The solvent dependence of the MOF will be of particular relevance in chapter 4 in which studies of the gas uptake properties of both the as-synthesised and $CHCl_3$-exchanged framework will be discussed.

3.6 References

1 A. Demessence, D. M. D'Alessandro, M. L. Foo, and J. R. Long, *J. Am. Chem. Soc.*, 2009, 131, 8784–8786.

2 B. Zheng, J. Bai, J. Duan, L. Wojtas, and M. J. Zaworotko, *J. Am. Chem. Soc.*, 2011, 133, 748–751.

3 S. Choi, T. Watanabe, T.-H. Bae, D. S. Sholl, and C. W. Jones, *J. Phys. Chem. Lett.*, 2012, 3, 1136–1141.

4 E. Neofotistou, C. D. Malliakas, and P. N. Trikalitis, *Chem. Eur. J*, 2009, 15, 4523–4537.

5 P. D. C. Dietzel, V. Besikiotis, and R. Blom, *J. Mater. Chem.*, 2009, 19, 7362-7370.

6 A. J. Fletcher, K. M. Thomas, and M. J. Rosseinsky, *J. Solid State Chem.*, 2005, 178, 2491–2510.

7 B. Yuan, D. Ma, X. Wang, Z. Li, Y. Li, H. Liu, and D. He, *Chem. Commun.*, 2012, 48, 1135–1137.

8 F. Millange, C. Serre, N. Guillou, G. Férey, and R. I. Walton, *Angew. Chemie Int. Ed.*, 2008, 47, 4100–4105.

9 Y.-S. Wei, K.-J. Chen, P.-Q. Liao, B.-Y. Zhu, R.-B. Lin, H.-L. Zhou, B.-Y. Wang, W. Xue, J.-P. Zhang, and X.-M. Chen, *Chem. Sci.*, 2013, 4, 1539-1546.

10 Y.-X. Tan, F. Wang, Y. Kang, and J. Zhang, *Chem. Commun.*, 2011, 47, 770–772.

11 S. Bourrelly, B. Moulin, A. Rivera, G. Maurin, S. Devautour-Vinot, C. Serre, T. Devic, P. Horcajada, A. Vimont, G. Clet, M. Daturi, J. C. Lavalley, S. Loera-Serna, R. Denoyel, P. L. Llewellyn, and G. Férey, *J. Am. Chem. Soc.*, 2010, 132, 9488–9498.

12 T. Devic, P. Horcajada, C. Serre, F. Salles, G. Maurin, B. Moulin, D. Heurtaux, G. Clet, A. Vimont, J.-M. Grenèche, B. Le Ouay, F. Moreau, E. Magnier, Y. Filinchuk, J. Marrot, J.-C. Lavalley, M. Daturi, and G. Férey, *J. Am. Chem. Soc.*, 2010, 132, 1127–36.

13 F. Millange, N. Guillou, M. E. Medina, G. Férey, A. Carlin-Sinclair, K. M. Golden, and R. I. Walton, *Chem. Mater.*, 2010, 22, 4237–4245.

14 R. I. Walton, A. S. Munn, N. Guillou, and F. Millange, *Chem. Eur. J.*, 2011, 17, 7069–7079.

15 A. B. Pangborn, M. a. Giardello, R. H. Grubbs, R. K. Rosen, and F. J. Timmers, *Organometallics*, 1996, 15, 1518–1520.

16 SMART APEX II, *Bruker AXS, Madison, Wisconsin, USA*.

17 R. H. Blessing, *Acta Crystallogr. A.*, 1995, 51, 33–38.

18 L. Krause, R. Herbst-Irmer, G. M. Sheldrick, and D. Stalke, *J. Appl. Cryst.*, 2015, 48, 3–10.

19 H. Nowell, S. a. Barnett, K. E. Christensen, S. J. Teat, and D. R. Allan, *J. Synchrotron Radiat.*, 2012, 19, 435–441.

20 O. V. Dolomanov, L. J. Bourhis, R. J. Gildea, J. a. K. Howard, and H. Puschmann, *J. Appl. Cryst.*, 2009, 42, 339–341.

21 G. M. Sheldrick, *Acta Crystallogr. A.*, 2008, 64, 112–22.

22 A. L. Spek, *Acta Crystallogr. D.*, 2009, 65, 148–55.

23 A. L. Spek, *Acta Crystallogr. C .*, 2015, 71, 9–18.

24 S. P. Thompson, J. E. Parker, J. Potter, T. P. Hill, A. Birt, T. M. Cobb, F. Yuan, and C. C. Tang, *Rev. Sci. Instrum.*, 2009, 80, 075107.

25 S. P. Thompson, J. E. Parker, J. Marchal, J. Potter, A. Birt, F. Yuan, R. D. Fearn, A. R. Lennie, S. R. Street, and C. C. Tang, *J. Synchrotron Radiat.*, 2011, 18, 637–648.

26 A. A. Coelho, *TOPAS Acad. Version 4.1, 2007, see http//www.topas-academic.net*.

27 A. A. Coelho, *J. Appl. Cryst.*, 2003, 36, 86–95.

28 G. S. Pawley, *J. Appl. Cryst.*, 1981, 14, 357–361.

29 H. M. Rietveld, *Acta Cryst.*, 1966, 20, 508–513.

30 H. M. Rietveld, *Acta Cryst.*, 1967, 22, 151–152.

31 H. M. Rietveld, *J. Appl. Cryst.*, 1969, 2, 65–71.

32 G. Chaplais, A. Simon-Masseron, F. Porcher, C. Lecomte, D. Bazer-Bachi, N. Bats, and J. Patarin, *Phys. Chem. Chem. Phys.*, 2009, 11, 5241-5245.

33 T. Loiseau, C. Serre, C. Huguenard, G. Fink, F. Taulelle, M. Henry, T. Bataille, and G. Férey, *Chem. Eur. J.*, 2004, 10, 1373–1382.

34 P. L. Llewellyn, S. Bourrelly, C. Serre, Y. Filinchuk, and G. Férey, *Angew. Chem. Int. Ed.*, 2006, 45, 7751–7754.

35 C. Serre, F. Millange, C. Thouvenot, M. Noguès, G. Marsolier, D. Louër, and G. Férey, *J. Am. Chem. Soc.*, 2002, 124, 13519–13526.

36 T. Loiseau, C. Mellot-Draznieks, H. Muguerra, G. Férey, M. Haouas, and F. Taulelle, *Comptes Rendus Chim.*, 2005, 8, 765–772.

37 I. Senkovska, F. Hoffmann, M. Fröba, J. Getzschmann, W. Böhlmann, and S. Kaskel, *Microporous Mesoporous Mater.*, 2009, 122, 93–98.

38 a. Schneemann, V. Bon, I. Schwedler, I. Senkovska, S. Kaskel, and R. a. Fischer, *Chem. Soc. Rev.*, 2014, 43, 6062–6096.

39 W.-P. Wu, Z.-S. Li, B. Liu, P. Liu, Z.-P. Xi, and Y.-Y. Wang, *Dalt. Trans.*, 2015, 44, 10141–10145.

40 Y. Chen, J. Zhang, J. Li, and J. V. Lockard, *J. Phys. Chem. C*, 2013, 117, 20068–20077.

41 J. Seo, C. Bonneau, R. Matsuda, M. Takata, and S. Kitagawa, *J. Am. Chem. Soc.*, 2011, 133, 9005–9013.